



# $\alpha$ -Synuclein kinetically regulates the nascent fusion pore dynamics

Rohith K. Nellikka<sup>a</sup>, Bhavya R. Bhaskar<sup>a</sup>, Kinjal Sanghrajka<sup>a</sup>, Swapnali S. Patil<sup>a</sup>, and Debasis Das<sup>a,1</sup>

<sup>a</sup>Department of Biological Sciences, Tata Institute of Fundamental Research, Mumbai 400005, India

Edited by Thomas C. Südhof, Stanford University, Stanford, CA, and approved July 13, 2021 (received for review October 17, 2020)

$\alpha$ -Synuclein ( $\alpha$ -syn<sub>FL</sub>) is central to the pathogenesis of Parkinson's disease (PD), in which its nonfunctional oligomers accumulate and result in abnormal neurotransmission. The normal physiological function of this intrinsically disordered protein is still unclear. Although several previous studies demonstrated  $\alpha$ -syn<sub>FL</sub>'s role in various membrane fusion steps, they produced conflicting outcomes regarding vesicular secretion. Here, we assess  $\alpha$ -syn<sub>FL</sub>'s role in directly regulating individual exocytotic release events. We studied the micromillisecond dynamics of single recombinant fusion pores, the crucial kinetic intermediate of membrane fusion that tightly regulates the vesicular secretion in different cell types.  $\alpha$ -Syn<sub>FL</sub> accessed v-SNARE within the trans-SNARE complex to form an inhibitory complex. This activity was dependent on negatively charged phospholipids and resulted in decreased open probability of individual pores. The number of trans-SNARE complexes influenced  $\alpha$ -syn<sub>FL</sub>'s inhibitory action. Regulatory factors that arrest SNARE complexes in different assembly states differentially modulate  $\alpha$ -syn<sub>FL</sub>'s ability to alter fusion pore dynamics.  $\alpha$ -Syn<sub>FL</sub> regulates pore properties in the presence of Munc13-1 and Munc18, which stimulate  $\alpha$ -SNAP/NSF-resistant SNARE complex formation. In the presence of synaptotagmin1 (syt1),  $\alpha$ -syn<sub>FL</sub> contributes with apo-syt1 to act as a membrane fusion clamp, whereas Ca<sup>2+</sup>•syt1 triggered  $\alpha$ -syn<sub>FL</sub>-resistant SNARE complex formation that rendered  $\alpha$ -syn<sub>FL</sub> inactive in modulating pore properties. This study reveals a key role of  $\alpha$ -syn<sub>FL</sub> in controlling vesicular secretion.

alpha-synuclein | fusion pore | membrane fusion | SNAREs

**P**arkinson's disease (PD) is a protein-misfolding disorder in which nonfunctional  $\alpha$ -syn<sub>FL</sub> oligomers accumulate within the cell. Several mutations in the gene encoding  $\alpha$ -syn<sub>FL</sub> are responsible for the dominantly inherited form of PD (1, 2), indicating a crucial role of  $\alpha$ -syn<sub>FL</sub> in disease pathogenesis. However, the normal cellular function of this intrinsically disordered protein is still unclear.

$\alpha$ -Syn<sub>FL</sub> is located at the neuronal cell body and presynaptic nerve terminal (3) and is suggested to be involved in synaptic vesicle trafficking (exo- and endocytosis) (4).  $\alpha$ -Syn<sub>FL</sub> overexpression in cultured hippocampal neurons and coronal slices showed miscellaneous spontaneous and evoked activities (4). Its overexpression, decreased evoking dopamine release from PC12 and chromaffin cells (5). Exocytosis of recycling endosomes was dependent on  $\alpha$ -syn<sub>FL</sub>'s differential expression in RBL-2H3 mast cells (6). It inhibited  $\alpha$ -granule secretion from platelets when stimulated with either ionomycin or thrombin (7).  $\alpha$ -Syn<sub>FL</sub> single-knockout (KO) mice of two age groups showed no effect in basal synaptic transmission (4); paired-pulse facilitation (PPF) remained unaltered in younger mice but reduced with age (4).  $\alpha/\beta/\gamma$ -Syn<sub>FL</sub> triple-KO (TKO) mice showed elevated basal synaptic transmission in young mice, unlike old mice, which showed a reduction in synaptic transmission (4, 8). PPF remained unaltered in hippocampal and corticostriatal slices of young  $\alpha/\beta/\gamma$ -syn<sub>FL</sub> TKO mice. All these previous studies suggest that  $\alpha$ -syn<sub>FL</sub> can affect cellular secretion from different cell types.

Cellular secretion involves the fusion of secretory vesicles with the plasma membrane in a spatiotemporally coordinated manner. In vitro reconstitution and cell-based studies showed that  $\alpha$ -syn<sub>FL</sub> interacts with the negatively charged phospholipids and

the v-SNARE (soluble N-ethylmaleimide-sensitive factor attachment protein receptor) synaptobrevin2 (syb2) (9, 10). Ensemble and single-molecule studies demonstrated  $\alpha$ -syn<sub>FL</sub>'s role in the docking step of membrane fusion (11) by cross-bridging v-SNAREs and acidic phospholipids (12).  $\alpha$ -Syn<sub>FL</sub> increased clustering of v-SNARE vesicles through its interaction with SNAREs and anionic lipids (13), a mechanism that explains how it engages secretory vesicles close to the active zone of the plasma membrane. It also affected the reclustering of synaptic vesicles (SVs) after endocytosis and thus resulted in reduced neurotransmitter release when overexpressed in hippocampal neurons (14). An in vitro lipid mixing assay also suggested inhibition of vesicle fusion by  $\alpha$ -syn<sub>FL</sub>'s direct interaction with lipid bilayers (15).  $\alpha$ -Syn<sub>FL</sub> was involved in priming ATP-induced exocytosis of secretory vesicles in PC12 cells and also affected the late stages of exocytosis (5, 16). Endogenous and overexpressed  $\alpha$ -syn<sub>FL</sub> was also found to promote fusion pore dilation and cargo discharge, while TKO increased pore closure in neurons and adrenal chromaffin cells (17, 18).

Although the above studies demonstrated  $\alpha$ -syn<sub>FL</sub>'s role in various steps of membrane fusion, they produced conflicting outcomes regarding vesicular secretion. Investigating the direct role of  $\alpha$ -syn<sub>FL</sub> on membrane fusion steps within the living cell was technically challenging. Furthermore, detailed in vitro studies using a defined system were limited by the time resolution to capture molecular events occurring in physiologically relevant time-scale (micromillisecond). To resolve this issue and to glean insight into  $\alpha$ -syn<sub>FL</sub>'s mode of action in micromillisecond time-scale, we used a recently described in vitro approach using v-SNARE-reconstituted nanodiscs (NDs) and t-SNARE-reconstituted black lipid membrane

## Significance

The accumulation of nonfunctional  $\alpha$ -synuclein ( $\alpha$ -syn<sub>FL</sub>) oligomers is the hallmark of Parkinson's disease (PD), affecting millions of people worldwide. Although  $\alpha$ -syn<sub>FL</sub> has a central role in PD, its cellular function is unclear until now. Understanding the normal function of  $\alpha$ -syn<sub>FL</sub> is critical to envisage the molecular basis of abnormal cellular secretion under disease conditions. Previous studies indicated that it can regulate various steps of membrane fusion. Fusion pores are the crucial kinetic intermediates during membrane fusion, through which vesicular secretion occurs from different cell types. Here, we describe a function of  $\alpha$ -syn<sub>FL</sub> in regulating the microsecond fusion pore transitions. This study offers an insight into how abnormal secretion occurs under pathological conditions in which nonfunctional  $\alpha$ -syn<sub>FL</sub> accumulates.

Author contributions: D.D. designed research; R.K.N., B.R.B., K.S., S.S.P., and D.D. performed research; R.K.N., B.R.B., K.S., and D.D. analyzed data; and R.K.N., B.R.B., K.S., and D.D. wrote the paper.

The authors declare no competing interest.

This article is a PNAS Direct Submission.

Published under the PNAS license.

<sup>1</sup>To whom correspondence may be addressed. Email: debasis.das@tifr.res.in.

This article contains supporting information online at <https://www.pnas.org/lookup/suppl/doi:10.1073/pnas.2021742118/-DCSupplemental>.

Published August 19, 2021.

(BLM) (19, 20). We investigated whether  $\alpha$ -syn<sub>FL</sub> regulates vesicular secretion by directly altering the microsecond transitions of individual exocytotic fusion pores (21).

During membrane fusion, the fusion pore is the crucial kinetic intermediate through which chemical messengers escape from the lumen of a secretory vesicle into the extracellular space (22). The principal components of exocytotic fusion pores are SNARE proteins (23, 24) and lipids (25). The cytoplasmic domains of v-SNAREs bind to the cognate domains on t-SNAREs, forming trans-SNARE complexes that catalyze the fusion pore formation and serve as the minimal machinery for membrane fusion (26, 27). On a microsecond time-scale, these ephemeral pores either close or dilate as the vesicle membrane fully collapses at the plasma membrane (21, 22, 28). Fusion pores are the site of action of many regulatory proteins that are known to stimulate or limit cellular secretion (29, 30). The ND-BLM system, mentioned above, has revealed that microsecond fusion pore transitions are controlled by the dynamic trans-SNARE complexes and the membrane lipid composition (19, 20). Here, we leverage the strength of this newly developed system to investigate the impact of  $\alpha$ -syn<sub>FL</sub> on fusion pore properties. Our single-pore measurements are supported by ensemble biochemical studies using v-SNARE NDs and t-SNARE liposomes.

$\alpha$ -Syn<sub>FL</sub> reduced the open probability of individual pores, without affecting the size of open pores. Open pore denotes the fully open state of a fusion pore unless mentioned otherwise. This observation prompted us to check whether it alters the trans-SNARE assembly. Interestingly,  $\alpha$ -syn<sub>FL</sub> enhanced trans-SNARE assembly as observed previously (10), and the effect was dependent on the presence of negatively charged phospholipids. Since  $\alpha$ -syn<sub>FL</sub> binds to both lipids (9, 31–33) and SNAREs (13, 34), we introduced strategies to decouple their contributions in regulating the pore properties. Lipid-binding of  $\alpha$ -syn<sub>FL</sub> stabilizes its interaction with the trans-SNARE complex and promotes the formation of an inhibitory trans complex. Since the number of trans complexes controls fusion pore properties (19), we investigated whether that impacts  $\alpha$ -syn<sub>FL</sub>'s functionality. The SNARE copy number directly influences  $\alpha$ -syn<sub>FL</sub>'s function of modulating fusion pore transitions. Next, we probed  $\alpha$ -syn<sub>FL</sub>'s pore modulatory capacity in presence of known regulatory factors that affect SNARE complex assembly during membrane fusion (30, 35, 36).  $\alpha$ -Syn<sub>FL</sub> significantly reduced the pore open probability in presence of Munc13-1 and Munc18, which organize a trans-SNARE assembly to produce an  $\alpha$ -SNAP/NSF-resistant complex (37–39). It assists syt1 to act as a membrane fusion clamp in absence of Ca<sup>2+</sup> (20, 40, 41). Upon Ca<sup>2+</sup> entry,  $\alpha$ -syn<sub>FL</sub> no longer elicits its inhibitory action and promotes syt1's function in dilating exocytotic fusion pores (20).

## Results

**$\alpha$ -Syn<sub>FL</sub> Kinetically Alters Fusion Pore Dynamics.** In cells, whether the effect of  $\alpha$ -syn<sub>FL</sub> on exocytosis results from the direct functional alteration of fusion pores is unclear. To address this, we first used an ND–liposome fusion assay (Fig. 1A) and measured glutamate release through fusion pores using an optical sensor for glutamate, iGluSnFR (25). NDs (13-nm diameter) bearing five copies of v-SNAREs (ND5) (19, 25, 42, 43) were allowed to react with the glutamate-entrapped t-SNARE liposomes (liposome-t), and glutamate release through the fusion pores was monitored in the absence and presence of increasing concentrations of  $\alpha$ -syn<sub>FL</sub> (Fig. 1B and C). We observed an approximately fivefold decrease in the glutamate release as we titrated from 0 to 10  $\mu$ M of  $\alpha$ -syn<sub>FL</sub> (Fig. 1B and C). The inhibitory effect on glutamate release was mediated by the monomeric  $\alpha$ -syn<sub>FL</sub> [ $\alpha$ -syn<sub>FL</sub> used in our experiments was purified by ion-exchange chromatography followed by gel filtration (SI Appendix, Fig. S1A and B), and the presence of monomeric  $\alpha$ -syn<sub>FL</sub> was confirmed by immunoblotting (SI Appendix, Fig. S1C)].  $\alpha$ -Syn<sub>FL</sub> alone did not produce detectable

leakage. Even a very high concentration of 100  $\mu$ M  $\alpha$ -syn<sub>FL</sub> failed to produce sulforhodamine B (SRB) loss from liposomes (SI Appendix, Fig. S1D).

Several cell-based and in vitro reconstitution studies have demonstrated a negative regulatory effect of  $\alpha$ -syn<sub>FL</sub> on vesicular secretion (4, 15), while a number of studies also demonstrated contrasting outcomes (4–7). To resolve this issue and to inspect whether  $\alpha$ -syn<sub>FL</sub> can directly modulate the micromillisecond dynamics of exocytotic fusion pores, we employed a recently described ND-BLM system (19, 20) (Fig. 1D and SI Appendix, Fig. S2) and studied the submillisecond dynamics of individual nascent fusion pores in absence and presence of  $\alpha$ -syn<sub>FL</sub>. When we used ND0 (ND bearing no syb2), 4  $\mu$ M  $\alpha$ -syn<sub>FL</sub> failed to produce any detectable effect on BLM (Fig. 1E, Upper). ND5, on the other hand, formed bonafide fusion pores, and the addition of the same amount of  $\alpha$ -syn<sub>FL</sub> caused a dramatic change in the pore properties, as we observed long closures of the individual pores (Fig. 1E, Lower). In all five trials, we observed repetitive transitions between open/partially open and closed states of pores before a final, stable, full closure. Current histograms as shown in Fig. 1F also confirmed the presence of distinct subconductance states followed by full closure. Diameters calculated from the conductance measurements (20) before and after  $\alpha$ -syn<sub>FL</sub> addition showed no alteration of the pore size (SI Appendix, Fig. S3). Further analysis revealed a significant reduction in the open-state stability in presence of 4  $\mu$ M  $\alpha$ -syn<sub>FL</sub>. The mean closed-state dwell times ( $\langle t_{c-obs} \rangle$ ) in the absence and presence of  $\alpha$ -syn<sub>FL</sub> were 0.006 ( $\pm$  0.002) s and 19.3 ( $\pm$  2.5) s, respectively. To gain insights into the number of kinetic steps during fusion pore transitions, the cumulative distribution functions (CDFs) of the closed-state dwell times were fitted with exponential functions (SI Appendix, Fig. S4A). Closed-time CDFs reflected the kinetics of fusion pores opening (20). In both the absence and presence of 4  $\mu$ M  $\alpha$ -syn<sub>FL</sub>, pore opening followed double exponential kinetics (SI Appendix, Fig. S4A), as described recently (20).  $\alpha$ -Syn<sub>FL</sub> significantly reduced the rate of fusion pores opening (SI Appendix, Fig. S4B). To calculate the open probability of individual pores, we performed additional kinetic analysis and quantified the fraction of time the individual pores occupied the closed state over a 30-min period of recording. We used a range of  $\alpha$ -syn<sub>FL</sub> concentrations from 0 to 10  $\mu$ M and quantified the above parameter from all these recordings (Fig. 1 and SI Appendix, Fig. S5). The “Fraction of time closed” ( $f_c$ ) increased with  $\alpha$ -syn<sub>FL</sub> concentration (Fig. 1G), having an EC<sub>50</sub> of  $3 \pm 0.5$   $\mu$ M. The pore open probability decreases with the increase in  $\alpha$ -syn<sub>FL</sub> concentration.

To check whether NDs' diameter influences  $\alpha$ -syn<sub>FL</sub>'s pore modulatory capacity, we reconstituted nine copies of v-SNAREs in a large  $\sim$ 30-nm ND (ND9<sub>L</sub>), described recently (20). A 10- $\mu$ M  $\alpha$ -syn<sub>FL</sub> significantly destabilized the fusion pore's open state with the appearance of long closures (SI Appendix, Fig. S6A) when ND9<sub>L</sub> was allowed to react with the t-SNAREs present in the BLM. In all three trials, we observed repetitive transitions between open/partially open and closed states before a final, stable, full closure. Current histograms also confirmed the presence of distinct subconductance states followed by the full closures (SI Appendix, Fig. S6B).  $\alpha$ -Syn<sub>FL</sub> addition showed a significant decrease in the pore open lifetime (SI Appendix, Fig. S6C). Hence, fusion pore transitions were kinetically altered in the presence of  $\alpha$ -syn<sub>FL</sub>, irrespective of whether v-SNAREs were reconstituted in small (ND5)- or large (ND9<sub>L</sub>)-size NDs.

Altogether, the above results suggest that  $\alpha$ -syn<sub>FL</sub> can directly alter micromillisecond dynamics of the fusion pore when minimal machinery was used to reconstitute the membrane fusion. It showed an inhibitory effect on vesicular secretion by altering the fusion pore kinetics. Next, we performed in-depth studies to investigate the cause of  $\alpha$ -syn<sub>FL</sub>-mediated fusion pore closure.

**$\alpha$ -Syn<sub>FL</sub> Localizes at the Membrane Fusion Site.**  $\alpha$ -Syn<sub>FL</sub> is localized at the presynaptic terminals (3). In human melanoma cells, it

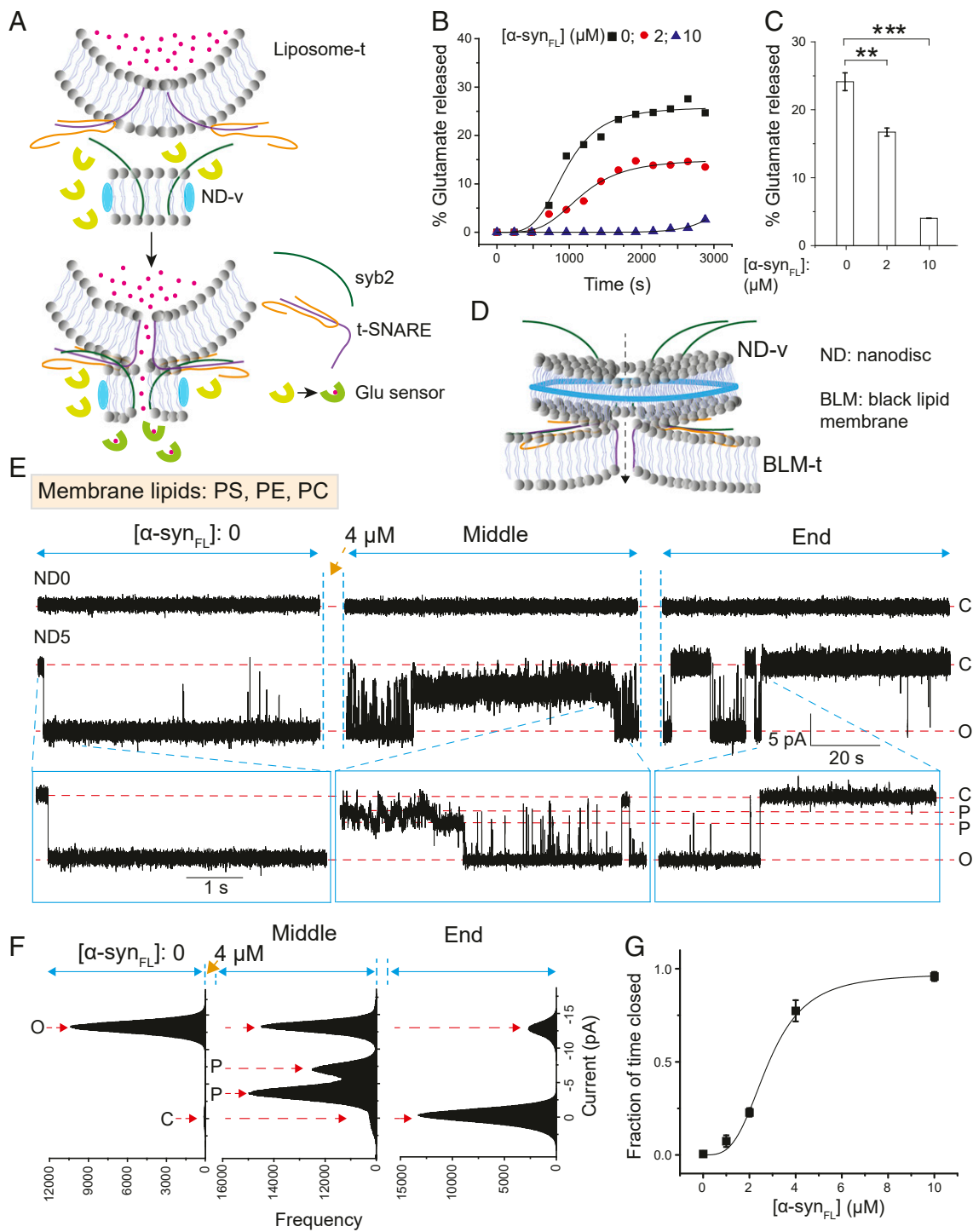


**Fig. 1.** Ensemble fusion assay and single-fusion pore measurements to trace  $\alpha$ -syn<sub>FL</sub>'s effect on membrane fusion. (A) Illustration summarizes the glutamate release assay. During fusion between ND-v (13-nm ND reconstituted with the v-SNARE syb2) and liposome-t (glutamate-entrapped t-SNARE liposomes), glutamate release through the fusion pores resulted in an increase in the fluorescence signal of the glutamate sensor (iGluSnFR), present in the reaction medium. (B) Time courses of glutamate release for experiments described in A, in absence and presence of different  $\alpha$ -syn<sub>FL</sub> concentrations. (C) Maximum percent (%) of glutamate release for the indicated conditions in B, are compared as bar graphs. Error bars indicate SEM from four independent trials under each of the conditions mentioned; three independent sets of NDs were used. The Student's *t* test was performed to compare the two means; \*\*\**p* < 0.001, \*\**p* < 0.01. (D) The illustration shows fusion pore formation as ND-v interacts with the BLM-t (t-SNAREs present in BLM). (E) Representative traces of single-fusion pores for ND0 (no syb2 in NDs) and ND5 (five copies of syb2 in NDs), in the absence and presence of  $\alpha$ -syn<sub>FL</sub>; experiments were performed using the ND-BLM system. Membrane lipid composition of both the NDs and BLMs is highlighted. An addition of 4  $\mu$ M  $\alpha$ -syn<sub>FL</sub> is indicated by the orange arrow. Full closed (C), partially open (P), and open (O) states of the individual pores are indicated along with the respective currents. (F) Current histograms of the ND5 pores from E, in absence and presence of 4  $\mu$ M  $\alpha$ -syn<sub>FL</sub>. Current distribution in different conducting states is shown. An addition of  $\alpha$ -syn<sub>FL</sub> is indicated by the orange arrow. (G) Fraction of time for which pores were fully closed (*f*<sub>c</sub>), plotted as a function of [ $\alpha$ -syn<sub>FL</sub>]. *n* = 5 independent BLMs; three sets of NDs were used (for 0, 1, and 4  $\mu$ M [ $\alpha$ -syn<sub>FL</sub>]). *n* = 3 independent BLMs; two sets of NDs were used (for 2 and 10  $\mu$ M [ $\alpha$ -syn<sub>FL</sub>]). Data are presented as mean  $\pm$  SEM.

colocalizes with the SNARE proteins syntaxin 1a and syb2 (33). To act on exocytotic fusion pores,  $\alpha$ -syn<sub>FL</sub> needs to be localized at the membrane fusion sites. Here, we first performed a cosedimentation assay (44) to validate the presence of  $\alpha$ -syn<sub>FL</sub> at the membrane fusion site (Fig. 2A). Immunoblots showed a significant amount of  $\alpha$ -syn<sub>FL</sub> copelleting with ND5 and t-SNARE liposomes when both the NDs and liposomes contained 1,2-dioleoyl-sn-glycero-3-phospho-l-serine (PS), 1,2-dioleoyl-sn-glycero-3-phosphoethanolamine (PE), and 1-Palmitoyl-2-oleoyl-sn-glycero-3-phosphocholine (PC) as the membrane lipids (Fig. 2B). The above observation can originate from  $\alpha$ -syn<sub>FL</sub>'s interaction with the negatively charged lipids as well as SNAREs. To disentangle the lipidic contribution, we omitted  $\alpha$ -syn<sub>FL</sub>'s known interacting partners PS and PE. We repeated the above assay with NDs and liposomes containing PC alone; the  $\alpha$ -syn<sub>FL</sub> level in the pellet reduced dramatically (Fig. 2B). The residual level of  $\alpha$ -syn<sub>FL</sub> under this condition could be originated due to its interaction with syb2.

We then quantified the amount of  $\alpha$ -syn<sub>FL</sub> bound to the membrane fusion site during trans complex formation using PS, PE, and PC.  $\alpha$ -Syn<sub>FL</sub> was mixed with ND5 and t-SNARE liposomes in different combinations (Fig. 2C). Ultracentrifugation should then pellet the membrane lipids along with the SNARE complexes and bound  $\alpha$ -syn<sub>FL</sub> (44). To quantify its localization during trans-SNARE complex formation, we then probed for unbound  $\alpha$ -syn<sub>FL</sub> in the supernatant, which proved lower than the input as it was bound to the membrane lipids and SNAREs (Fig. 2C, Lower).  $\alpha$ -Syn<sub>FL</sub> was bound to t-SNARE liposomes containing PS and PE, as evident from its reduced level in the supernatant (Fig. 2C, Lower). ND5 alone did not appear in the pellet significantly, as evidenced from the immunoblot of syb2 (SI Appendix, Fig. S7A), and hence, we were unable to assess the

fraction of  $\alpha$ -syn<sub>FL</sub> bound to ND5 alone. When ND5 was engaged in trans complex formation with t-SNARE liposomes, it appeared in the pellet as demonstrated by immunoblots of syb2 and syntaxin 1a of the pellet (Fig. 2C, Upper and SI Appendix, Fig. S7A). Interestingly, under that condition, we observed maximum decrease of  $\alpha$ -syn<sub>FL</sub> level in the supernatant (Fig. 2C, Lower) and with a concomitant increase in the pellet (Fig. 2C, Upper). Quantification yielded a significant increase of  $\alpha$ -syn<sub>FL</sub>-bound fraction when ND5 was engaged in trans complex formation (Fig. 2D). Finally, we studied the effect of  $\alpha$ -syn<sub>FL</sub> on the trans-SNARE complex assembly. An ND5/t-SNARE liposome fusion assay demonstrated an approximately twofold increase in SNARE complex formation in presence of 4  $\mu$ M  $\alpha$ -syn<sub>FL</sub> (10) (Fig. 2E).

Together, these results indicate that  $\alpha$ -syn<sub>FL</sub> remains bound to the membrane fusion site through its interaction with phospholipids and SNAREs.  $\alpha$ -Syn<sub>FL</sub>'s membrane interaction within the time frame of our experiments does not induce its oligomerization (SI Appendix, Fig. S7B).

**Membrane-Binding of  $\alpha$ -syn<sub>FL</sub> Promotes Its Functional Interaction with the Trans-SNARE Complex.**  $\alpha$ -Syn<sub>FL</sub> is a 140-amino acid protein with two functionally important regions. Its N terminus forms an  $\alpha$ -helix and is essential for binding to phospholipid membranes (32), whereas the acidic C terminus interacts with SNAREs (10, 34) (Fig. 3A). To glean detailed insight into  $\alpha$ -syn<sub>FL</sub>'s mode of action, we attempted to decouple the roles of N and C terminus in controlling fusion pore dynamics.

First, we omitted PS and PE from the ND5 and BLM, leaving PC as the only lipid used for these experiments. Interestingly, in our planar bilayer recordings with PC alone, 4  $\mu$ M  $\alpha$ -syn<sub>FL</sub> failed to elicit considerable changes in the individual pore's properties

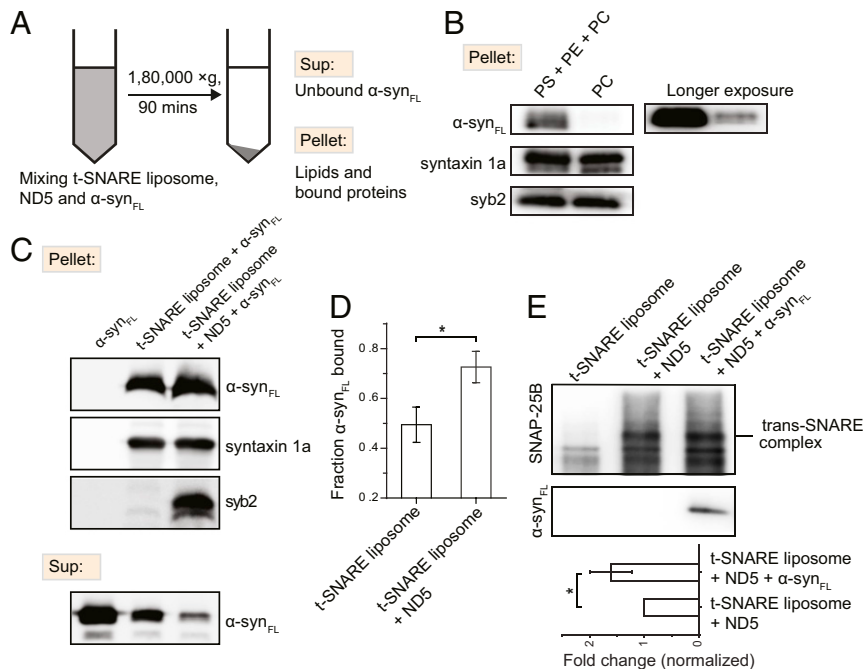


**Fig. 2.**  $\alpha$ -Syn<sub>FL</sub>'s localization at the membrane fusion site and its effect on SNARE complex assembly. (A) The schematic shows cosedimentation assay to determine  $\alpha$ -syn<sub>FL</sub>'s presence at the membrane fusion site. (B) Representative immunoblots showing the presence of  $\alpha$ -syn<sub>FL</sub> with syb2 and syntaxin 1a in the pellet, in the absence and presence of the negatively charged phospholipids (PS and PE).  $n = 3$  independent experiments. (C, Upper) Representative immunoblot of syb2 and syntaxin 1a in the pellet fractions under the indicated conditions. (Lower) Representative immunoblot of  $\alpha$ -syn<sub>FL</sub> in the corresponding supernatant fractions. Membrane lipid compositions used in these sets of experiments were PS, PE, and PC. (D) Fraction of  $\alpha$ -syn<sub>FL</sub> bound under indicated conditions are quantified from C and plotted as bar graphs.  $n = 4$  independent experiments; data are presented as mean  $\pm$  SEM. The Student's  $t$  test was performed to compare the two means,  $*p < 0.05$ . (E, Upper Middle) Representative immunoblots for SNAP-25B and  $\alpha$ -syn<sub>FL</sub> showing trans-SNARE complex under indicated conditions. (Lower) Pooled results to indicate normalized fold change, plotted as bar graphs, to compare the effect of 4  $\mu$ M  $\alpha$ -syn<sub>FL</sub> on trans-SNARE complex formation.  $n = 4$  independent experiments; data are presented as mean  $\pm$  SEM. The Student's  $t$  test was performed to compare the two means,  $*p < 0.05$ .

(Fig. 3B).  $\langle t_{c-obs} \rangle$  in absence and presence of  $\alpha$ -syn<sub>FL</sub> were 0.005 ( $\pm 0.0007$ ) s and 0.006 ( $\pm 0.003$ ) s, respectively, indicating that  $\alpha$ -syn<sub>FL</sub> had no significant effect on closed-state stability. The current histogram showed that PS and PE are required for  $\alpha$ -syn<sub>FL</sub> to elicit its action on fusion pores, as the pores mostly occupied the open state (Fig. 3C). The open-state dwell-time distribution in absence of  $\alpha$ -syn<sub>FL</sub> showed predominantly longer open lifetimes (Fig. 3D). The addition of  $\alpha$ -syn<sub>FL</sub> did not affect the longer open-lifetime distribution; however, a minor increase in the shorter open lifetime was observed (Fig. 3D). Hence,  $\alpha$ -syn<sub>FL</sub>'s interaction with negatively charged phospholipids is a crucial determinant for its action on nascent fusion pores.

To assess the importance of its SNARE-binding domain in regulating pore properties, we then used an  $\alpha$ -syn<sub>FL</sub> C-terminal-derived peptide ( $\alpha$ -syn<sub>91-140</sub>), which, according to previous studies (10, 34), should primarily interact with SNAREs (Fig. 4A). A 4- $\mu$ M  $\alpha$ -syn<sub>91-140</sub> induced significant changes in pore properties when PC was used as the only membrane lipid (SI Appendix, Fig. S8). Pores transitioned between open/partially open and closed states (SI Appendix, Fig. S8), and current histograms showed increased closed and subconductance state occupancy (SI Appendix, Fig. S8). Open-state lifetime distributions showed a significant decrease in an open lifetime in the presence of this peptide (SI Appendix, Fig. S8). However, none of our repetitions using this peptide yielded stable, full pore closure.

We then included PS and PE in NDs and BLM.  $\alpha$ -syn<sub>91-140</sub> produced similar effects on pores as observed above in absence of these negatively charged phospholipids (Fig. 4B). Pores transitioned between distinct open/partially open and closed states

(Fig. 4B), further confirmed by the current histograms (Fig. 4C). Open-state lifetime distributions also shifted substantially to the shorter lifetime (Fig. 4D). Again, none of our repetitions using this peptide yielded stable full pore closure, which was observed with  $\alpha$ -syn<sub>FL</sub> under the same condition (Fig. 1E). We presume that the observed pore properties in the presence of  $\alpha$ -syn<sub>91-140</sub> resulted from its interaction with syb2 within the functional trans-SNARE complexes. It is to be noted that these trans complexes were found to be dynamic (19). Adding the cytoplasmic domain of syb2 could also access the trans-SNARE complexes and alter the fusion pore dynamics (19, 20).

We performed the reciprocal experiments using only the lipid-binding domain of  $\alpha$ -syn<sub>FL</sub> ( $\alpha$ -syn<sub>1-90</sub>), in presence of PS, PE, and PC as the membrane lipids. The addition of 4  $\mu$ M  $\alpha$ -syn<sub>1-90</sub> did not produce a detectable change in the pore properties (SI Appendix, Fig. S9A); current histograms showed mostly open-state occupancy (SI Appendix, Fig. S9B). Open-lifetime distribution didn't alter considerably (SI Appendix, Fig. S9C).

Together, the above results indicate that while bound to the membrane through its membrane-binding domain,  $\alpha$ -syn<sub>FL</sub> can modulate the nascent fusion pore by interacting with syb2 present within the trans-SNARE complex. Membrane lipid composition plays a crucial role in  $\alpha$ -syn<sub>FL</sub> function. The membrane-bound  $\alpha$ -syn<sub>FL</sub> was found to be conformationally more dynamic than the free  $\alpha$ -syn<sub>FL</sub> (33).

$\alpha$ -Syn<sub>FL</sub> is known to be a curvature-sensing protein (45). Since we are using NDs in our experiments, we deliberated whether the effect of  $\alpha$ -syn<sub>FL</sub> on trans-SNARE dynamics is limited by the ND curvature. Because liposomes contain more curved surfaces

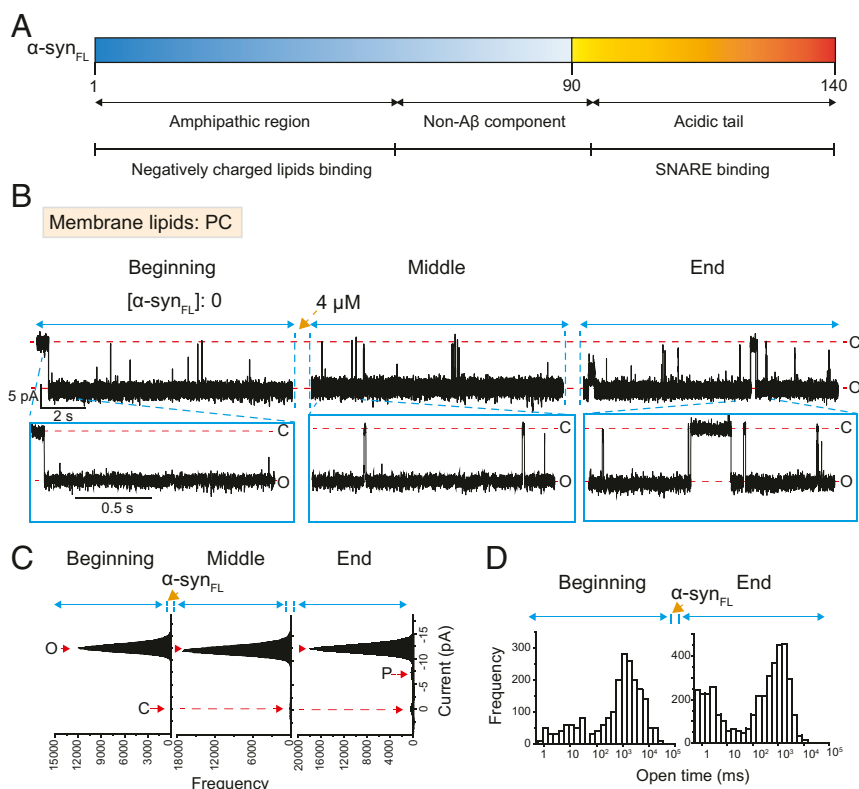


**Fig. 3.** Negatively charged phospholipids regulate  $\alpha$ -syn<sub>FL</sub>'s function on fusion pore transitions. (A) Cartoon shows the domains of  $\alpha$ -syn<sub>FL</sub>. Corresponding amino acid numbers are mentioned in the illustration. (B) Representative trace showing the effect of  $\alpha$ -syn<sub>FL</sub> on a single pore formed using ND5, with PC alone as the membrane lipid in NDs and BLM. An addition of 4  $\mu$ M  $\alpha$ -syn<sub>FL</sub> is indicated by the orange arrow. Closed (C) and open (O) states of the individual pore are indicated along with the current and time scales. (C) Current histograms of the ND5 pores from B in the absence and presence of 4  $\mu$ M  $\alpha$ -syn<sub>FL</sub> are compared. The current distribution in different conducting states is shown for the beginning, middle, and end of the traces. An addition of  $\alpha$ -syn<sub>FL</sub> is indicated by the orange arrow. (D) Open dwell-time histograms of pores in absence and presence of  $\alpha$ -syn<sub>FL</sub> under indicated conditions in B. An addition of  $\alpha$ -syn<sub>FL</sub> is indicated by the orange arrow.  $n = 5$  independent BLMs for each of the experimental conditions; three sets of NDs were used.

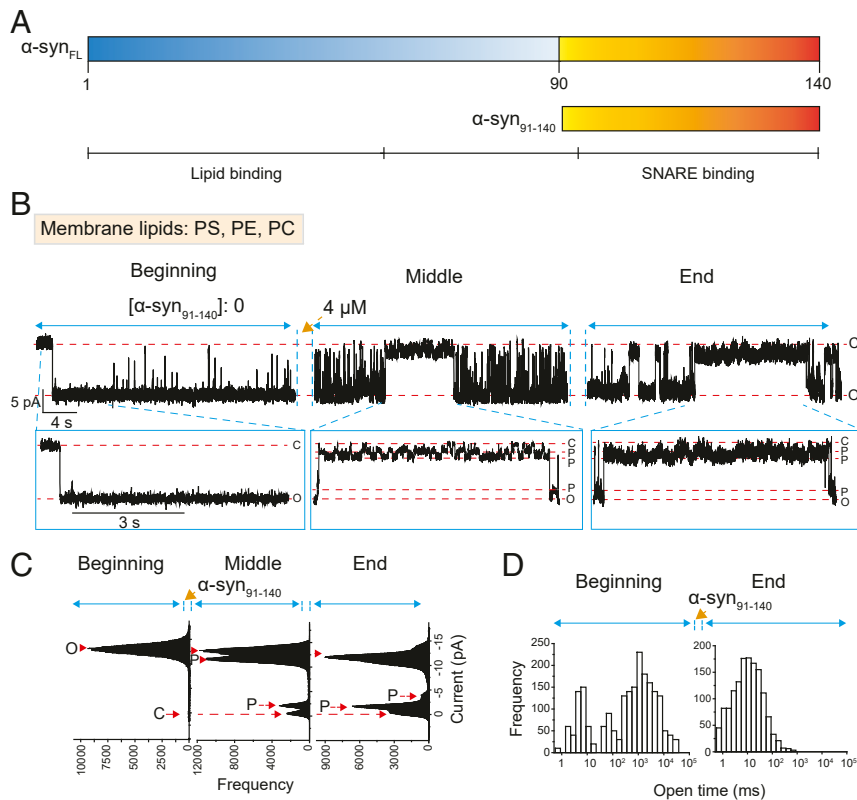


**Fig. 4.** Role of  $\alpha$ -syn<sub>FL</sub>'s SNARE-binding domain in regulating fusion pore properties. (A) Cartoon shows the peptide  $\alpha$ -syn<sub>91-140</sub>, derived from  $\alpha$ -syn<sub>FL</sub>. Corresponding amino acid numbers are mentioned in the illustration. (B) Representative trace showing the effect of  $\alpha$ -syn<sub>91-140</sub> peptide on a single pore formed using ND5, with PS, PE, and PC as the membrane lipids in NDs and BLM. An addition of 4  $\mu$ M  $\alpha$ -syn<sub>91-140</sub> is indicated by the orange arrow. Full closed (C), partially open (P), and open (O) states of the individual pore are indicated along with the current and time scales. (C) Current histograms of the ND5 pores from B in the absence and presence of  $\alpha$ -syn<sub>91-140</sub> are compared. Current distribution in different conducting states is shown for the beginning, middle, and end of the traces. An addition of  $\alpha$ -syn<sub>91-140</sub> peptide is indicated by the orange arrow. (D) Open dwell-time histograms of pores in absence and presence of  $\alpha$ -syn<sub>91-140</sub>. Addition of  $\alpha$ -syn<sub>91-140</sub> is indicated by the orange arrow.  $n = 5$  independent BLMs for each of the experimental conditions; three sets of NDs were used.

than NDs, we compared the efficiency of trans complex formation during ND–liposome and liposome–liposome fusion. We used Glomelt dye that yields enhanced fluorescence upon binding to the exposed hydrophobic regions of proteins. When a protein folds into a compact structure, the dye is expelled out of the hydrophobic region, producing a decrease in the Glomelt fluorescence (46). Here, we used this assay to probe for the impact of membrane curvature on trans complex formation. v-SNAREs were reconstituted in either NDs or liposomes, whereas t-SNAREs were reconstituted in only liposomes (SI Appendix, Fig. S10A). The addition of dye to t-SNARE liposomes in the presence of ND5 or v-SNARE liposomes resulted in an enhanced fluorescence at the time ( $t$ ) = 0, which decreased with time as the transcomplexes formed. A corresponding increase in the fraction of t-SNAREs bound to v-SNAREs was quantified from here (SI Appendix, Fig. S10B), which was larger in NDs compared to liposomes. This difference could originate because ~20 to 30% of v-SNAREs were oriented toward the lumen of the liposomes, as described previously (47), rendering them inaccessible for complex formation. To account for the dye binding to other components of the reaction (other than SNAREs), we used empty NDs and liposomes (Methods).  $\alpha$ -Syn<sub>FL</sub> was not used directly in the above Glomelt assay, as that might produce composite results regarding SNARE assembly. When SNARE complexes were allowed to form overnight at 4 °C, v-SNAREs reconstituted in NDs and liposomes were equally capable of forming SNARE complexes, as evidenced by immunoblotting (SI Appendix, Fig. S10C). Immunoblots showed enhanced trans complex formation in presence of  $\alpha$ -syn<sub>FL</sub>, when v-SNAREs were reconstituted into NDs (Fig. 2E). A similar

observation was also reported when v-SNAREs were reconstituted into liposomes (10). Hence, in our experiments,  $\alpha$ -syn<sub>FL</sub>-mediated modulation of trans-SNARE dynamics is not affected by membrane curvature.

**Number of Trans-SNARE Complexes Directly Influence  $\alpha$ -syn<sub>FL</sub>'s Activities on Fusion Pores.** A synaptic vesicle contains ~70 copies of syb2 (48), whereas only approximately two to three copies may be sufficient for fusion (42, 49). The number of trans-SNARE complexes has been found to modulate the size and kinetic properties of individual pores (19). As demonstrated above,  $\alpha$ -syn<sub>FL</sub> altered the fusion pore properties, presumably by interacting with the trans complexes. Here, we asked whether its function is affected by the SNARE copy numbers.

We first used a limiting  $\alpha$ -syn<sub>FL</sub> concentration of 1  $\mu$ M and used two different ND preparations, constituting syb2 copy numbers of 4 and 7 (i.e., ND4 and ND7, 13-nm diameters). With this limiting concentration,  $\alpha$ -syn<sub>FL</sub> was able to elicit significant effects on pore properties in the case of ND4 (Fig. 5A, Upper), producing  $\langle t_{c-obs} \rangle$  of 2 ( $\pm$  0.12) s. Three out of nine trials with ND4 yielded partial open states in the presence of 1  $\mu$ M  $\alpha$ -syn<sub>FL</sub> (SI Appendix, Fig. S11A). Pores formed using ND7 under this condition showed a significant reduction in  $\alpha$ -syn<sub>FL</sub> efficacy as compared to ND4 (Fig. 5A, Lower), and  $\langle t_{c-obs} \rangle$  was 0.005 ( $\pm$  0.0006) s. ND7 pores under this condition did not show any partial open states. Hence, the appearance of the pore subconductance states, as shown above (Fig. 1E and F), was  $\alpha$ -syn<sub>FL</sub> concentration and SNARE copy number dependent. Current histograms in Fig. 5B showed a drastic change in the closed-state currents of

ND4 pores in presence of 1  $\mu\text{M}$   $\alpha\text{-syn}_{\text{FL}}$ . ND7 pores under this condition showed no considerable changes in the closed-state currents (Fig. 5B). We performed an in-depth kinetic analysis to compare the closed-time distributions of ND4 and ND7 pores (Fig. 5C). ND4 pores in absence of  $\alpha\text{-syn}_{\text{FL}}$  showed a shorter closed-state lifetime distribution (Fig. 5C, Upper), while the presence of 1  $\mu\text{M}$   $\alpha\text{-syn}_{\text{FL}}$  shifted the distribution predominantly to the longer lifetime (Fig. 5C, Lower). In the absence of  $\alpha\text{-syn}_{\text{FL}}$ , ND7 pores showed shorter closed-time distribution compared to ND4 (Fig. 5C, Upper). The addition of the same amount of  $\alpha\text{-syn}_{\text{FL}}$  to ND7 pores showed no significant alteration in closed-time distribution (Fig. 5C, Lower). To measure the open probability, next, we quantified the  $f_c$ . This value decreased in presence of 1  $\mu\text{M}$   $\alpha\text{-syn}_{\text{FL}}$ , as we increased the syb2 copy numbers in the NDs from 4 to 7 (Fig. 5D).

Finally, 4- $\mu\text{M}$   $\alpha\text{-syn}_{\text{FL}}$  showed stable, full pore closures in the case of ND4 (SI Appendix, Fig. S11 B, Upper). ND7 pores under this condition showed predominantly subconductance states, indicative of partial opening of pores (SI Appendix, Fig. S11 B, Lower). A higher 10- $\mu\text{M}$  concentration of  $\alpha\text{-syn}_{\text{FL}}$  produced full, stable closure of ND7 pores (SI Appendix, Fig. S12).

Altogether, these results indicate that the number of trans-SNARE complexes directly influences  $\alpha\text{-syn}_{\text{FL}}$ 's function. It stoichiometrically interacts with syb2 within the trans complex. Similar expression of  $\alpha\text{-syn}_{\text{FL}}$  inside the cell might elicit different effects on exocytotic fusion pores, formed by a different number of SNAREs (5, 8, 10, 50–56).

**Regulatory Factors Differentially Alter  $\alpha\text{-syn}_{\text{FL}}$ 's Pore Modulatory Capacity.** Cellular secretion is regulated by accessory factors, which act on different steps of membrane fusion and control the amount of cargo release (29, 30). We next probed for  $\alpha\text{-syn}_{\text{FL}}$ 's ability to modulate fusion pore dynamics in presence of regulatory factors that organize SNARE complex assembly.

At first, we used a combination of Munc13-1 (Munc13-1 fragment spanning C1, C2B, MUN, and C2C domains) (57) and Munc18, which assemble SNAREs to form an  $\alpha\text{-SNAP/NSF}$ -resistant complex (37–39).  $\alpha\text{-Syn}_{\text{FL}}$  enhanced trans-SNARE assembly when ND5 was allowed to react with t-SNARE liposomes in presence of Munc13-1 and Munc18 (SI Appendix, Fig. S13). In the ND-BLM experiments,  $\alpha\text{-syn}_{\text{FL}}$  significantly destabilized the pore open states in presence of these Munc proteins (SI Appendix, Fig. S14A). In both the absence and presence of 4  $\mu\text{M}$   $\alpha\text{-syn}_{\text{FL}}$ , pore opening followed double exponential kinetics, as evidenced by the fitting of closed-time CDFs (SI Appendix, Fig. S14B).  $\alpha\text{-Syn}_{\text{FL}}$  significantly reduced the rate of pore opening under this condition (SI Appendix, Fig. S14C), indicating its ability to kinetically regulate pore dynamics in presence of Munc13-1 and Munc18.

The vesicular release is thought to be triggered by the binding of  $\text{Ca}^{2+}$  ions to syt1, in the case of LDCVs (Large Dense Core Vesicles) and SVs (35, 36, 58–60). In contrast, apo-syt1 acts as a fusion clamp, which is associated with syt1's ability to drive the assembly of trans-SNARE complexes into a more zippered yet inhibited state (20, 40, 41). Next, we explored whether  $\alpha\text{-syn}_{\text{FL}}$  can elicit its pore regulatory capacity in presence of syt1.

We reconstituted full-length syt1 along with syb2 into 13 nm NDs (ND4/syt1, SI Appendix, Fig. S15) and used the ND-BLM system to study the properties of individual pores. As observed in Fig. 6A (Upper, Left), the pores remained mostly closed in absence of  $\text{Ca}^{2+}$ . This recapitulated the syt1-mediated clamping phenotype of fusion pores as observed previously (20). Addition of 4- $\mu\text{M}$   $\alpha\text{-syn}_{\text{FL}}$  stabilized the closed state significantly (Fig. 6A, Upper, Right), as  $\langle t_{\text{c-obs}} \rangle$  shifted from 0.03 ( $\pm 0.005$ ) s (in the case of no  $\alpha\text{-syn}_{\text{FL}}$ ) to 3.2 ( $\pm 0.08$ ) s (in the case of 4- $\mu\text{M}$   $\alpha\text{-syn}_{\text{FL}}$ ). However, the size of open pore was not altered by  $\alpha\text{-syn}_{\text{FL}}$ , as the conductance measurements didn't change considerably (SI Appendix, Fig. S16).

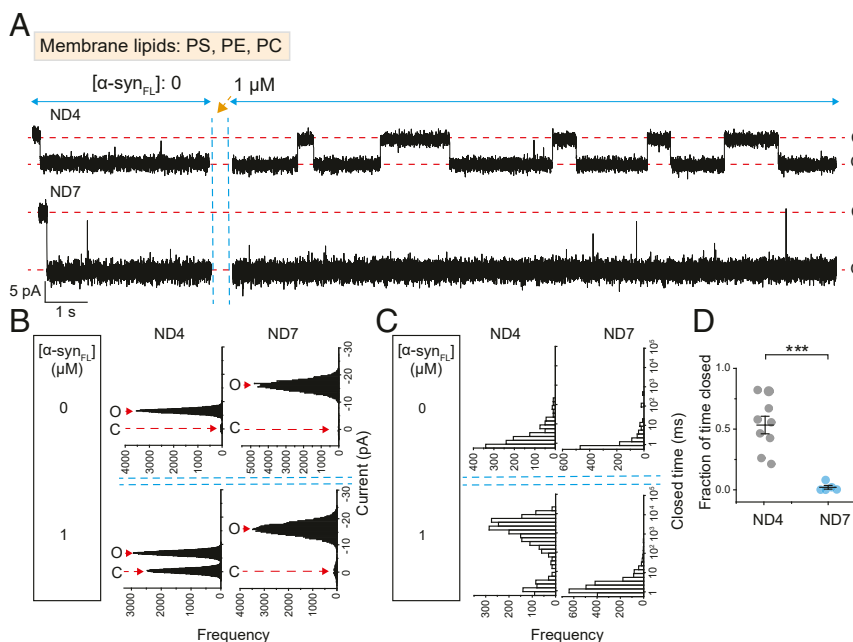


**Fig. 5.** SNARE copy numbers influence  $\alpha\text{-syn}_{\text{FL}}$ 's functionality. (A) Representative traces showing the effect of 1  $\mu\text{M}$   $\alpha\text{-syn}_{\text{FL}}$  on single pores formed by ND4 (Upper) and ND7 (Lower). Closed (C) and open (O) states are indicated along with the current and time-scale. An addition of 1  $\mu\text{M}$   $\alpha\text{-syn}_{\text{FL}}$  is indicated by the orange arrow. (B) Current histograms of the pores from A, in absence and presence of  $\alpha\text{-syn}_{\text{FL}}$ . Closed (C) and open (O) states are indicated by red arrows. (C) Closed dwell-time histograms of ND4 and ND7 pores in the absence (Upper) and presence (Lower) of 1  $\mu\text{M}$   $\alpha\text{-syn}_{\text{FL}}$  are shown.  $n = 9$ , and 5 independent BLMs for ND4 and ND7, respectively; three sets of NDs were used. (D) Fraction of time for which pores were fully closed ( $f_c$ ) in presence of 1  $\mu\text{M}$   $\alpha\text{-syn}_{\text{FL}}$  are plotted as a function of syb2 copy numbers in NDs.  $n = 9$ , and 5 independent BLMs for ND4 and ND7, respectively; three sets of NDs were used. The Student's  $t$  test was performed to compare the two means,  $***p < 0.001$ . Data are shown as mean  $\pm$  SEM.

The addition of  $\text{Ca}^{2+}$  to the pores formed by ND4/syt1 resulted in pore dilation with stable open states (20) (Fig. 6 *A*, Lower, Left and *SI Appendix*, Fig. S16). Strikingly, the same concentration of  $\alpha\text{-syn}_{\text{FL}}$  did not change either the kinetic properties or size of open pores (Fig. 6 *A*, Lower, Right and *SI Appendix*, Fig. S16).  $\langle t_{\text{c-obs}} \rangle$  values in absence (0.006  $\pm$  0.001) s and presence (0.008  $\pm$  0.0007) s of 4- $\mu\text{M}$   $\alpha\text{-syn}_{\text{FL}}$  didn't alter significantly, and the effects were not  $[\text{Ca}^{2+}]_{\text{free}}$  dependent (*SI Appendix*, Fig. S17). Further increase of  $\alpha\text{-syn}_{\text{FL}}$  concentration also had no detectable effect (*SI Appendix*, Fig. S18).  $\alpha\text{-Syn}_{\text{FL}}$  remained in a monomeric state in presence of 0.5 mM  $[\text{Ca}^{2+}]_{\text{free}}$  in our experimental system (*SI Appendix*, Fig. S19).

We also quantified the open probability of pores under different conditions (as measured by  $f_c$ ). The addition of 4- $\mu\text{M}$   $\alpha\text{-syn}_{\text{FL}}$  in apo-syt1 condition increased  $f_c$  significantly compared to no  $\alpha\text{-syn}_{\text{FL}}$  (Fig. 6*B*), indicating that it further decreased the open probability. In contrast,  $\alpha\text{-syn}_{\text{FL}}$  was unable to elicit significant changes in the open probabilities after  $\text{Ca}^{2+}$ •syt1 triggered the pores to dilate (Fig. 6*B*). Our detailed kinetic analysis confirmed the appearance of long closures in the presence of  $\alpha\text{-syn}_{\text{FL}}$  under the apo-syt1 condition (Fig. 6*C*, Upper). In the presence of  $\text{Ca}^{2+}$ , it failed to elicit significant change in the closed-time distribution (Fig. 6 *C*, Lower). As observed previously (20), this  $\text{Ca}^{2+}$ •syt1-triggered opening could be reversed in the presence of ATPase NSF, with the help of  $\alpha\text{-SNAP}$ , which closed the pores irreversibly (*SI Appendix*, Fig. S20). Thus, the  $\text{Ca}^{2+}$  switch that activates syt1 to induce vesicular release from LDCVs and SVs concomitantly deactivates  $\alpha\text{-syn}_{\text{FL}}$  to elicit its inhibitory action on fusion pores.

To test whether the ND diameter influences  $\alpha\text{-syn}_{\text{FL}}$ 's pore modulatory action in case of regulated secretion, we reconstituted full-length syt1 along with syb2 into ~30-nm NDs (ND9<sub>L</sub>/syt1) (20). Under the apo-syt1 condition, individual pores remained mostly in the closed states, recapitulating syt1's clamping activity (*SI Appendix*, Fig. S21*A*). The detailed kinetic analysis confirmed the appearance of long closures in presence of  $\alpha\text{-syn}_{\text{FL}}$  (*SI Appendix*, Fig. S21*B*). It considerably reduced the open probability under the apo-syt1 condition. Hence, under the apo-syt1 condition, fusion pore transitions were kinetically altered in presence of  $\alpha\text{-syn}_{\text{FL}}$ , irrespective of whether syb2 and syt1 were reconstituted in small (ND5)- or large (ND9<sub>L</sub>)-size NDs. When  $\text{Ca}^{2+}$ •syt1 triggered the pores to dilate in larger conductance states (*SI Appendix*, Fig. S21*A*), a 10- $\mu\text{M}$   $\alpha\text{-syn}_{\text{FL}}$  remained ineffective in altering pore properties. The kinetic analysis revealed no noticeable change in the pore properties upon  $\alpha\text{-syn}_{\text{FL}}$  addition (*SI Appendix*, Fig. S21*B*). Hence, under the  $\text{Ca}^{2+}$ -triggered condition, fusion pore transitions remained unaltered in presence of  $\alpha\text{-syn}_{\text{FL}}$ , regardless of whether syb2 and syt1 were reconstituted in small- or large-size NDs.

Together, the above results suggest that  $\alpha\text{-syn}_{\text{FL}}$ 's pore regulatory capacity is dependent on the physiological conditions, at which regulatory factors clamp SNARE complexes in different assembly states. These results can explain some conflicting outcomes regarding  $\alpha\text{-syn}_{\text{FL}}$ 's role in regulated secretion from different cell types, as mentioned above.

## Discussion

$\alpha\text{-Syn}_{\text{FL}}$  is abundantly expressed in neuronal cells and less abundantly in other tissues, such as the heart, skeletal muscle, pancreas, and placenta (7). Its overexpression and KO studies showed conflicting outcomes on spontaneous and evoked release from different cell types (e.g., neurons, neuroendocrine cells, platelets, and RBL-2H3 mast cells) (4–7). Abnormal dopamine release has direct consequences in PD, in which nonfunctional  $\alpha\text{-syn}_{\text{FL}}$  oligomers accumulate (61, 62). The release of chemical messengers involves the fusion of secretory vesicles with the plasma membrane in a spatiotemporally coordinated manner. In vitro reconstitution and cell-based studies, which attempted to demonstrate  $\alpha\text{-syn}_{\text{FL}}$ 's role in membrane fusion steps, produced contrasting results regarding vesicular secretion (5, 10–18). To resolve this issue and to

glean detailed insight into  $\alpha\text{-syn}_{\text{FL}}$ 's mode of action, we used an ND-liposome-based reconstitution approach and a recently described ND-BLM system to study the effect of  $\alpha\text{-syn}_{\text{FL}}$  on a crucial membrane fusion intermediate—the fusion pores.

$\alpha\text{-Syn}_{\text{FL}}$  inhibited glutamate release through the pores when minimal fusion machinery was reconstituted in the NDs and liposomes (Fig. 1). A titration of  $[\alpha\text{-syn}_{\text{FL}}]$  showed a gradual decrease of glutamate release with the increasing  $[\alpha\text{-syn}_{\text{FL}}]$  (Fig. 1*C*). In this assay, the v-SNAREs in both the sides of NDs are available to fuse with the t-SNARE liposomes, which might result in a sandwich of liposome–ND–liposome. This arrangement would not allow liposome-entrapped glutamate to release into the medium; hence, considerably less glutamate would be available to interact with the iGluSnFR. However, the read-out of our iGluSnFR-based content release assay yielded comparable membrane fusion efficiency as previously reported, in which v- and t-SNAREs were reconstituted in two different liposomes (26, 63) or NDs and liposomes (42). Hence, in our experimental conditions and time frame, the large population of t-SNARE liposomes presumably interacts with one side of the NDs.

The ND-BLM system allowed us to probe for  $\alpha\text{-syn}_{\text{FL}}$ 's direct effect in regulating micromillisecond dynamics of fusion pores (Fig. 1 and *SI Appendix*, Fig. S6). The reduced-pore open probability in presence of  $\alpha\text{-syn}_{\text{FL}}$  (Fig. 1 and *SI Appendix*, Fig. S6) offers a direct explanation for  $\alpha\text{-syn}_{\text{FL}}$ -mediated negative regulatory effect on spontaneous secretion, observed in cell-based and reconstitution studies (4, 15). Nevertheless, it also contradicted many studies that probed for  $\alpha\text{-syn}_{\text{FL}}$ 's role in spontaneous and evoked release (4–7).

To clarify this, we next performed in-depth studies and assessed the cause of  $\alpha\text{-syn}_{\text{FL}}$ -mediated fusion pore closure. First, we asked whether  $\alpha\text{-syn}_{\text{FL}}$  enhances the SNARE complex assembly, as observed previously (10). Indeed,  $\alpha\text{-syn}_{\text{FL}}$  promoted the SNARE complex assembly in our experimental system (Fig. 2*E*).  $\alpha\text{-Syn}_{\text{FL}}$ 's role in clustering the membranes through its interaction with SNAREs and anionic lipids (13), might promote this assembly. Chemical cross-linking showed that a multimeric form of  $\alpha\text{-syn}_{\text{FL}}$  is responsible for promoting the assembly (64).

Next, we designed strategies to dissect the role of  $\alpha\text{-syn}_{\text{FL}}$ 's lipid- and SNARE-binding activities (10, 13, 34) in regulating fusion pore properties. Our results indicated that  $\alpha\text{-syn}_{\text{FL}}$ 's inhibitory effect on modulating pore dynamics requires the presence of both the lipid- and SNARE-binding domains. Presumably,  $\alpha\text{-syn}_{\text{FL}}$  exists in an autoinhibitory form while it is not associated with the membrane. Membrane-binding induces a conformational change (33), which allows it to stably interact with syb2 in the functional trans-SNARE complex. This stimulates the inhibitory trans complex formation (Fig. 6*D*). Although  $\alpha\text{-syn}_{\text{FL}}$  is a curvature-sensing protein (45), NDs used in our experiments do not limit  $\alpha\text{-syn}_{\text{FL}}$  in promoting inhibitory trans complex formation. Our experiments suggested that NDs and liposomes are equally efficient in producing trans-SNARE complexes (*SI Appendix*, Fig. S10). Thus, the curvature sensitivity of  $\alpha\text{-syn}_{\text{FL}}$  did not come into play in these actions.

The above experiments using minimal machinery provided valuable information that  $\alpha\text{-syn}_{\text{FL}}$  can access v-SNAREs in the dynamic trans-SNARE complex and regulate the pore properties. The number of trans complexes engaged in a fusion pore assembly has a profound impact on pore size and kinetic properties (19, 20). We simultaneously altered SNARE copy numbers and  $\alpha\text{-syn}_{\text{FL}}$  concentration and discovered that  $\alpha\text{-syn}_{\text{FL}}$ 's pore modulatory capacity is dependent on its stoichiometric interaction with the v-SNAREs in the dynamic trans complex (Fig. 5 and *SI Appendix*, Figs. S11 and S12). This suggests that the effect of endogenous  $\alpha\text{-syn}_{\text{FL}}$  on vesicular secretion might be dependent on its expression level, as reported in a recent study (6).  $\alpha\text{-Syn}_{\text{FL}}$ 's similar expression can induce different effects on vesicular secretion when the different number of trans-SNAREs are engaged in fusion pore assembly.



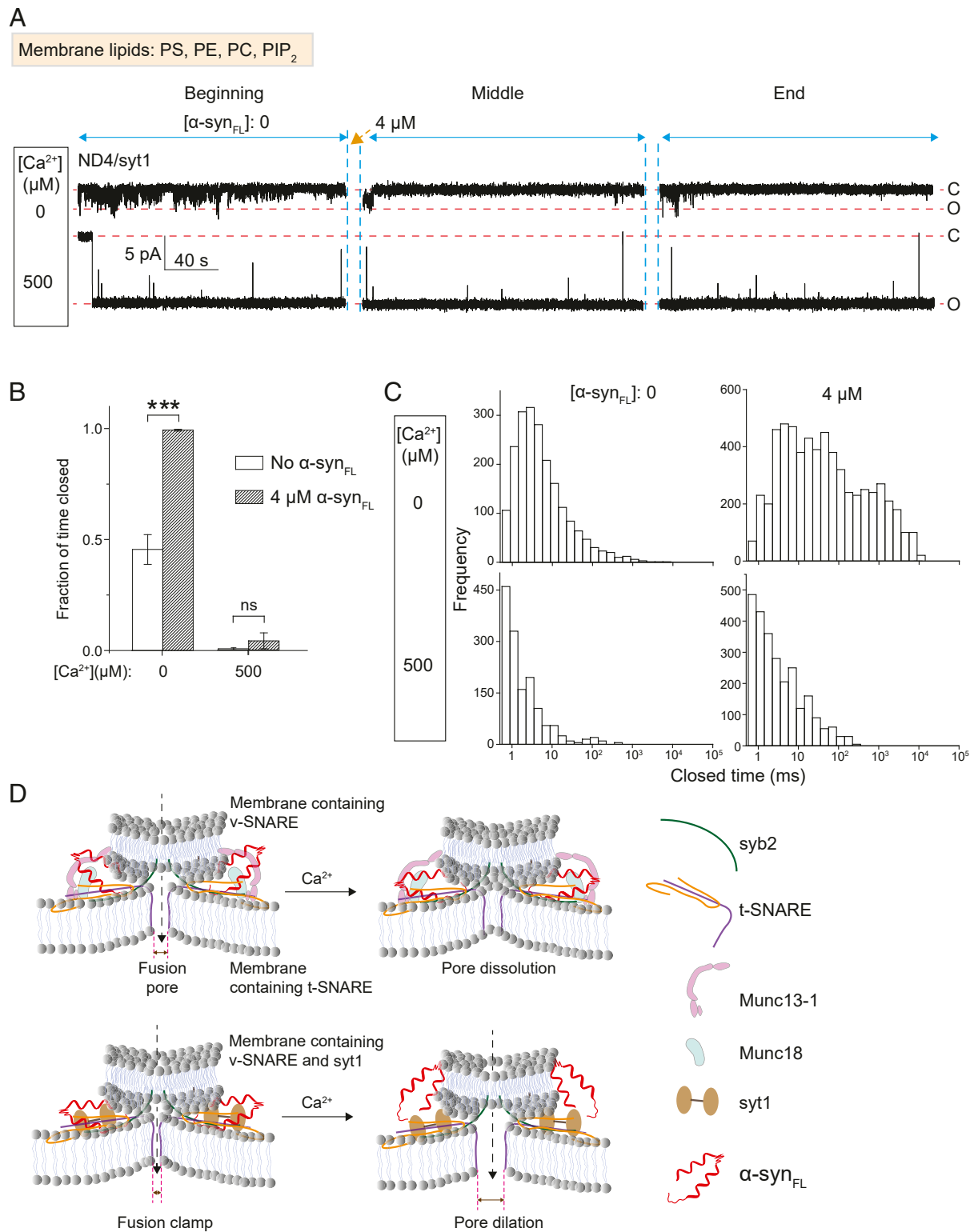


**Fig. 6.** Regulatory factors differentially control  $\alpha$ -syn<sub>FL</sub>'s function. (A) Traces of single pores with/without  $\alpha$ -syn<sub>FL</sub> are shown for ND4/syt1. In each trace, minus (–) Ca<sup>2+</sup> contains 1 mM BAPTA (in all ND-BLM experiments using syt1), and plus (+) Ca<sup>2+</sup> contains 500  $\mu$ M [Ca<sup>2+</sup>]<sub>free</sub>. An addition of 4  $\mu$ M  $\alpha$ -syn<sub>FL</sub> is indicated by the orange arrow. Closed (C) and open (O) states are shown; the current and time-scale, for all traces, is shown in the inset. (B) Fraction of time for which pores were fully closed ( $f_c$ ) under indicated conditions is plotted as bar graphs.  $n = 4$  independent BLMs for each of the conditions; three sets of NDs.  $***p < 0.001$ ,  $ns: p > 0.05$ , Kruskal–Wallis  $U$  test, and Tukey's multiple comparison tests. Data are shown as mean  $\pm$  SEM. (C) Closed-state, dwell-time histograms for indicated conditions are shown.  $n = 5$  independent BLMs under each condition; three sets of NDs were used. (D) Schematic describing the mode of action of  $\alpha$ -syn<sub>FL</sub> in regulating the nascent fusion pores. (Upper)  $\alpha$ -syn<sub>FL</sub> stimulates pore dissolution in presence of Munc13-1 and Munc18. (Lower)  $\alpha$ -syn<sub>FL</sub> in absence of Ca<sup>2+</sup> facilitates syt1's function to act as fusion clamp; under stimulated condition, Ca<sup>2+</sup> influx inactivates  $\alpha$ -syn<sub>FL</sub>'s function and promotes syt1 mediated pore dilation.

Downloaded at Palestinian Territory, occupied on December 6, 2021

To better mimic the physiological situation, we investigated  $\alpha$ -syn<sub>FL</sub>'s pore modulatory capacity in presence of known regulatory factors. Since  $\alpha$ -syn<sub>FL</sub> elicited its action through trans-SNARE complexes, we used two classes of factors that regulate membrane fusion by acting on trans complexes. Munc13-1 and Munc18 stimulate the formation of  $\alpha$ -SNAP/NSF-resistant trans complex (37–39).  $\alpha$ -Syn<sub>FL</sub> enhanced trans-SNARE assembly in presence of these Munc proteins (*SI Appendix, Fig. S13*) and acted on that complex to disassemble fusion pore, leading to its closure (*SI Appendix, Fig. S14* and Fig. 6D). Munc13-1 possesses an elongated structure in absence of membrane or SNAREs (65). It is still unknown whether it adopts the same structure in the presence of donor and acceptor membranes during trans-SNARE assembly. In this study, we have used NDs with a 13-nm diameter to investigate the pore modulatory role of  $\alpha$ -syn<sub>FL</sub> in presence of Munc13-1 and Munc-18. Further studies using larger-size NDs might provide additional insight into this mechanism.

Syt1 in absence of Ca<sup>2+</sup> also acts as a membrane fusion clamp through its action on trans complexes (20, 40, 41).  $\alpha$ -Syn<sub>FL</sub> acted on that complex and contributed significantly to stabilize a fusion pore closed state (Fig. 6 and *SI Appendix, Fig. S21*). In presence of Ca<sup>2+</sup>, syt1 induces additional trans-SNARE zippering toward C-terminal, which can be disassembled by  $\alpha$ -SNAP/NSF (20, 40, 41) (*SI Appendix, Fig. S20*). Ca<sup>2+</sup>•syt1 thus drives the formation of a large, stable open-fusion pore (20, 40, 41) (Fig. 6);  $\alpha$ -syn<sub>FL</sub> is unable to alter that pore's properties (Fig. 6 and *SI Appendix, Fig. S21*). These results indicate that stimulated conditions can result in the formation of an  $\alpha$ -syn<sub>FL</sub>-resistant trans complex. This renders  $\alpha$ -syn<sub>FL</sub> inactive to modulate pore transitions, as indicated by previous cell-based studies in which no  $\alpha$ -syn<sub>FL</sub>-mediated effect on evoked release was observed (4). Based on different SNARE assembly states, organized by different regulatory factors,  $\alpha$ -syn<sub>FL</sub>'s pore modulatory capacity alters inside the cell. Further cell-based studies are needed to clarify these results.

In this study, we investigated  $\alpha$ -syn<sub>FL</sub>'s pore modulatory capacity in presence of a limited number of regulatory factors. The inclusion of crucial proteins like complexins, NSF,  $\alpha$ -SNAP, etc. in the reconstitution will provide further insight into  $\alpha$ -syn<sub>FL</sub>'s action. Overexpression (66–68) and in vitro reconstitution studies (69, 70) demonstrated complexin to be a clamp for membrane fusion. Evidence also suggests that membrane fusion starts with syntaxin-1a•Munc18-1 complex. Munc18-1/Munc13-1 orchestrate fusion together with SNAREs and Ca<sup>2+</sup>•syt1 in an NSF- and  $\alpha$ -SNAP-resistant manner (37). Future reconstitutions using these accessory proteins will reveal interesting insights into  $\alpha$ -syn<sub>FL</sub>'s function.

Overall, our current study demonstrated a function of  $\alpha$ -syn<sub>FL</sub> in regulating micromillisecond dynamics of exocytotic fusion pores. It will initiate research to understand how nonfunctional  $\alpha$ -syn<sub>FL</sub> oligomers, under pathological conditions, alter the cellular secretion of chemical messengers.

## Methods

**Materials.** PE, PC, PS, 1-palmitoyl-2-oleoyl-sn-glycero-3-phospho-(1'-rac-glycerol) (sodium salt) (PG), and brain Phosphatidylinositol 4,5-bisphosphate or PtdIns(4,5)P<sub>2</sub> (PI(4,5)P<sub>2</sub>) were purchased from Avanti polar lipids; DDM (n-dodecyl  $\beta$ -D-maltoside) and OG (n-octyl glucoside) were from Gold Biotechnology; IPTG (Isopropyl  $\beta$ -D-1-thiogalactopyranoside), Triton X 100, and DEAE Sephadex were from Sigma-Aldrich; Glutathione Sepharose 4 B and Ni-Sepharose 6 Fast Flow were from GE Healthcare; 2-mercaptoethanol and glycerol were from Thermo Fischer Scientific; and Bio-Beads SM2 were from BIO-RAD. The  $\alpha$ -Syn<sub>91–140</sub> peptide was synthesized, purified, and analyzed by mass spectrometry at Genscript. The  $\alpha$ -Syn<sub>1–90</sub> fragment was cloned and purified as a GST-tagged protein. Rat Munc13-1 (spanning C1, C2B, MUN, and C2C domains) (57) for bacterial expression was a kind gift from Prof. Josep Rizo. The antibodies used in this study are listed in *SI Appendix, Table S1*.

**Protein Purification.** Complementary DNA for the following proteins was derived from rat-neuronal SNAREs (syb2, syntaxin-1a, and SNAP-25B), syt1, NSF, and  $\alpha$ -SNAP (20, 25, 71).

Syb2, t-SNARE heterodimers comprising syntaxin-1a, and SNAP-25B were expressed at 37 °C, and syt1 was expressed at 28 °C; these were purified as his<sub>6</sub>-tagged proteins, as described previously (20, 25, 71), with some modifications. Bacterial pellets were resuspended (~10 mL per liter of culture) in resuspension buffer (25 mM Hepes-KOH pH 7.4, 400 mM KCl, 10 mM imidazole, and 5 mM  $\beta$ -mercaptoethanol). Protease inhibitor mixture, EDTA-free (Roche) DNase I, and RNase (Sigma, 10  $\mu$ g/mL) were then added, and samples were sonicated in 35-mL batches on ice for 6  $\times$  15 seconds (20% duty cycle). Triton X-100 was added to 2.1% (vol/vol) and incubated overnight with rotation at 4 °C before centrifugation of the cell lysate at 14,000 rpm for 30 min in a JA-17 rotor (Eppendorf). The supernatant was then incubated for >2 h at 4 °C with Ni-NTA agarose (GE Healthcare; 0.5 mL of a 50% slurry per liter of cell culture) equilibrated in resuspension buffer. Beads were washed extensively with resuspension buffer containing 1% Triton X-100 and then washed with OG wash buffer (25 mM Hepes-KOH pH 7.4, 400 mM KCl, 10 mM imidazole, 10% glycerol, 5 mM  $\beta$ -mercaptoethanol, and 1% OG). The slurry was loaded onto a column, washed with five to 10 column volumes of OG wash buffer and step-eluted with OG wash buffer containing 500 mM imidazole. The purity of proteins was assessed using sodium dodecyl sulphate–polyacrylamide gel electrophoresis (SDS-PAGE) after staining with Coomassie brilliant blue.

MSPE3D1, NW30,  $\alpha$ -SNAP, NSF, iGluSnFR, Munc13-1, and Munc18 were also purified as his<sub>6</sub>-tagged proteins, as described previously (20, 25). In brief, a similar procedure as above was used to purify these proteins except all detergents were omitted from the wash buffers. The purified proteins were dialyzed against 25 mM Hepes-KOH (pH 7.4), 100 mM KCl, 10% glycerol, and 1 mM dithiothreitol (DTT).

$\alpha$ -Syn<sub>FL</sub> was purified using a method described previously (72, 73), with necessary modifications. In brief, a plasmid containing mouse  $\alpha$ -syn<sub>FL</sub> was expressed in *Escherichia coli* BL21(DE3) cells and induced with 0.5 mM IPTG for 4 h at 37 °C. The cells were pelleted, washed, and sonicated with resuspension buffer (10 mM Tris-Cl pH 7.4, 5 mM NaCl, protease inhibitor mixture, DNase I, and RNase). The supernatant following sonication was loaded onto a DEAE Sepharose column and eluted using elution buffer (10 mM Tris-Cl pH 7.4 and 300 mM NaCl). To isolate monomeric  $\alpha$ -syn<sub>FL</sub>, gel filtration was carried out using a Superdex 200 10/300 GL column, equilibrated in reconstitution buffer 25 mM Hepes-KOH pH 7.4, 100 mM KCl, and 1 mM DTT). The purity of monomeric  $\alpha$ -syn<sub>FL</sub> was assessed by immunoblot, using a monoclonal  $\alpha$ -syn<sub>FL</sub> antibody.

**Proteoliposome Reconstitution.** v- and t-SNARE liposomes were prepared as described previously (19). In brief, syb2 or t-SNARE heterodimers were mixed with lipids in reconstitution buffer (25 mM Hepes-KOH, pH 7.5, 100 mM KCl, and 1 mM DTT) plus 0.02% OG. The following lipid compositions were used in different experiments: 1) 100% PC; 2) 32% PE, 52% PC, 16% PS; 3) 30% PE, 52% PC, 16% PS, 2% PIP<sub>2</sub>; 4) 75% PE, 25% PG; 5) 31% PE, 51% PC, 15% PS, 1.5% PIP<sub>2</sub>, and 1.5% DAG. Dialysis was performed against reconstitution buffer (overnight, 4 °C), followed by the isolation of t-SNARE liposomes by flotation using ACCUDENZ gradient. For this purpose, ultracentrifugation was performed at 180,000  $\times$  g for 2 h in Optima MAX-XP ultracentrifuge (Beckman Coulter). Glutamate-entrapped t-SNARE liposomes are designated as "liposome-t"; empty liposomes harboring t-SNAREs are designated as "t-SNARE liposomes."

**ND Reconstitution.** Reconstitution of syb2 into NDs was performed as described previously (19, 43). In some experiments, full-length syt1 was reconstituted with syb2 at a 1:3 (syt1:syb2) molar ratio, as described previously (20). MSP1E3D1 and NW30 were used to generate 13- and ~30-nm NDs. The ratios of membrane scaffolding protein (MSP) to lipid molecules used were 3:180 (for 13-nm NDs) and 2:1,000 (for ~30-nm NDs); while the MSP to syb2 ratios were 3:3 (ND4), 3:6 (ND5), and 3:9 (ND7). The syb2 and syt1 copy numbers per ND refer to the total number of syb2 and syt1 molecules, not the number of copies per face of the ND. The following lipid compositions were used as indicated: 1) 16% PS, 32% PE, 52% PC; 2) 100% PC; 3) 40% PS, 15% PE, 45% PC; and 4) 31% PE, 51% PC, 15% PS, 1.5% PIP<sub>2</sub>, and 1.5% DAG. Briefly, reconstitution involved mixing syb2, MSP, and lipids, with or without syt1 in reconstitution buffer containing 0.02% DDM. Detergent was slowly removed with Bio-Beads (1/3 volume) with gentle shaking (overnight, 4 °C). The NDs in the supernatant were purified by gel filtration using a Superdex 200 10/300 GL column, equilibrated in reconstitution buffer.

**Ensemble Fusion Assay.** Ensemble fusion assays were performed with the glutamate sensor iGluSnFR (1  $\mu$ M) (25, 42), ND5 (0.2  $\mu$ M), and liposome-t (0.004  $\mu$ M) in the absence or presence of  $\alpha$ -syn<sub>FL</sub> of the indicated amount. The glutamate release upon membrane fusion activated iGluSnFR to produce enhanced fluorescence, which was monitored for 1 h in a plate reader

(Tecan Infinite M200). After each run, 5  $\mu\text{L}$  of 5% Triton X-100 was added to each reaction, and data were collected for another 25 min.

**SRB Assay.** SRB (20 mM) incorporated t-SNARE liposomes were prepared as described earlier (74). SRB-incorporated t-SNARE liposomes (0.004  $\mu\text{M}$ ) were incubated in the absence or presence of increasing  $[\alpha\text{-syn}_{\text{FL}}]$ . SRB release from liposomes was recorded by the characteristic fluorescence emission for 1 h (Excitation 532-nm; Emission 586 nm). After each recording, 5  $\mu\text{L}$  of 5% Triton X-100 was added to each reaction, and data were collected for another 20 min.

**Planar Lipid Bilayer Electrophysiology.** Planar lipid bilayer (BLM) recordings were performed using a Planar Lipid Bilayer Workstation from Warner Instruments (19, 20, 75, 76). Briefly, lipids (as indicated, at 30 mg/mL in *n*-decane) were first painted onto a 150- $\mu\text{m}$  aperture in a 1-mL polystyrene cup (Warner Instruments) and dried for 10 min. After that, the aperture was immersed in 1 mL of 25 mM Hepes-KOH, pH 7.4 with 100 mM KCl in the cis and 10 mM KCl in the trans chamber. Silver-silver chloride electrodes were connected to each chamber. The lipid solution was gently reapplied to the hole until a conductance-blocking seal was formed, as determined by capacitance. This process was repeated, either with a brush or air bubble until the desired capacitance was achieved.

**Single-Fusion Pore Measurements.** Single-pore measurements were performed using the methods described before (19, 20). Briefly, after the formation of BLM, t-SNARE proteoliposomes were added to the cis chamber, which spontaneously fused with the planar bilayer, thus depositing the t-SNAREs into the BLM. t-SNAREs were reconstituted into BLMs, at a density of 0.4 molecules per  $\mu\text{m}^2$  (20). Then, to form fusion pores, v-SNARE NDs (reconstituted with/without syt1) were added to the cis chamber. Pores formed within 5 to 30 min and could be monitored for  $\geq 90$  min. Currents were recorded using Bilayer Clamp Amplifier BC-535 (Warner Instrument) and a Digidata 1550B (with Humsilencer) acquisition system (Molecular Devices Corp.) in the absence and presence of the indicated amount of  $\alpha\text{-syn}_{\text{FL}}$  or an  $\alpha\text{-syn}_{\text{FL}}$ -derived peptide,  $\alpha\text{-syn}_{91-140}$ . Single-channel recordings were acquired at 10 kHz using pCLAMP 11 (Molecular Devices, LLC.) software and were filtered at 5 kHz using a multisection Bessel filter.  $\Delta\psi \equiv \psi_{\text{cis}} - \psi_{\text{trans}}$  ( $\psi_{\text{trans}} \equiv 0$  V). All recordings were conducted at room temperature. Pore formation and dynamics were studied at  $\Delta\psi = -50$  mV.

When syt1 was used, experiments were initiated with 1 mM BAPTA in the cis chamber, followed by the sequential addition of reconstituted liposomes bearing t-SNAREs and then NDs and subsequently the indicated amount of  $\alpha\text{-syn}_{\text{FL}}$ . In another set, the addition of 1 mM BAPTA, t-SNARE liposomes, and v-SNARE NDs was followed by the addition of 1.5 mM  $\text{CaCl}_2$  in the cis chamber, which yielded  $[\text{Ca}^{2+}]_{\text{free}}$  of 500  $\mu\text{M}$ . The indicated concentration of  $\alpha\text{-syn}_{\text{FL}}$  was added after that. In the experiments where Munc13-1 and Munc18 were used, BLMs contained PS, PE, PC, PIP<sub>2</sub>, and DAG.

To study the effect of PS and PE on  $\alpha\text{-syn}_{\text{FL}}$ 's action, NDs and BLM lipid composition were varied as indicated in the text. BLMs were formed following the same technique as described in *Planar Lipid Bilayer Electrophysiology*.

To study the effect of  $\alpha\text{-SNAP}$ , NSF, ATP, and  $\text{Mg}^{2+}$ , the indicated concentration of each factor was added to the cis chamber, after pores had opened.

**Analysis of Single-Fusion Pore Unitary Currents.** Single-channel data were analyzed using Clampfit 10.7 (Molecular Devices, LLC.) and MS Origin 2018 (OriginLab). In all figures showing BLM recordings, the representative traces were filtered at 1 kHz for display purposes.

Current histograms were plotted using CLAMPFIT 10.7 and fitted with Gaussian functions. To calculate the open lifetime of individual pores, 30-min recordings of individual traces were analyzed. Dwell times corresponding to the fully open and fully closed states were measured in individual records using the event detector in CLAMPFIT10.7. Closed-state, dwell-time histograms were plotted using MS Origin 2018 (OriginLab).

The fraction of time fully closed ( $f_c$ ) was calculated using the equation:

$$\text{Fraction of time closed} = \frac{\text{closed dwell time}}{\text{open dwell time} + \text{closed dwell time}}$$

**Kinetic Analysis of Single-Pore Data.** Kinetic analysis of single-channel data was performed using previously reported methods (20). Closed-state dwell times ( $\langle t_{\text{c-obs}} \rangle$ ) were detected in CLAMPFIT 10.7. These were further statistically analyzed by CDFs [defined by the probability  $P(t_{\text{closed}} \leq t)$ ] using Origin 2018. Closed-state CDFs of individual traces were fitted with the different exponential fits, and the goodness of fit was determined using Akaike

Information Criterion (77, 78), as described previously (20). CDFs generated from the closed-state dwell times provided kinetics for the pore opening.

**Immunoblotting.** Immunoblotting was performed by mixing the samples with 1 $\times$  (final concentration) Laemmli sample buffer and heated at 95  $^{\circ}\text{C}$  for 5 min. Samples were run on SDS-PAGE and blotted onto a polyvinylidene difluoride membrane. The membrane was blocked with 5% skimmed milk in Tris-buffered saline containing 0.1% Tween 20 (TBS-T) and incubated with respective primary antibodies (*SI Appendix, Table S1*) overnight at 4  $^{\circ}\text{C}$ . The blots were washed with TBS-T and incubated with corresponding horseradish peroxidase-conjugated secondary antibody (*SI Appendix, Table S1*) for 1 h at room temperature. The blots were developed using enhanced chemiluminescence. For SNARE complex detection, samples were prepared without boiling.

**Cosedimentation Assay.** This assay was performed following a reported protocol (44), with necessary modifications. t-SNARE liposomes alone or in combination with ND5 (equal number of t- and v-SNAREs were allowed to react) were incubated overnight at 4  $^{\circ}\text{C}$  with  $\alpha\text{-syn}_{\text{FL}}$  in a 100  $\mu\text{L}$  reaction, using reconstitution buffer (25 mM Hepes-KOH pH-7.4, 100 mM KCl, and 1 mM DTT). The liposomes, as well as trans-SNARE complexes, were then pelleted by centrifuging at 180,000 g for 90 min at 4  $^{\circ}\text{C}$ . Both the supernatant and pellet were probed for SNAREs and  $\alpha\text{-syn}_{\text{FL}}$  in different experiments, using respective monoclonal antibodies. The  $\alpha\text{-syn}_{\text{FL}}$  band intensities in the supernatant corresponded to the unbound fraction. Fraction  $\alpha\text{-syn}_{\text{FL}}$  bound to the lipids, and SNAREs were calculated with respect to the input  $\alpha\text{-syn}_{\text{FL}}$  in the control lane. ImageJ software was used to quantify the band intensities. The pellet samples were probed with syntaxin 1a and syb2 to verify the presence of t-SNAREs and ND5, respectively, in the trans-SNARE complex.

**Quantitation of SNARE Complexes in Western Blot.** Equal concentrations of t-SNARE liposomes and ND5 were incubated with or without 4  $\mu\text{M}$   $\alpha\text{-syn}_{\text{FL}}$  in reconstitution buffer (25 mM Hepes-KOH pH-7.4, 100 mM KCl, and 1 mM DTT) overnight at 4  $^{\circ}\text{C}$ . The samples were probed with both  $\alpha\text{-syn}_{\text{FL}}$  and SNAP-25 antibodies in the immunoblots. The blots were analyzed using ImageJ software and the amount of SNARE complex formation was quantified by measuring the band intensities after background correction, under indicated conditions.

**Glomelt Assay to Trace SNARE Complex Formation.** Glomelt dye (0.2 $\times$  final concentration) was mixed with t-SNARE liposomes and v-SNARE NDs or liposomes in a reaction buffer containing 25 mM Hepes-KOH pH 7.4, 100 mM KCl, and 1 mM DTT. Fluorescence intensity was monitored for 1 h in a plate reader (Tecan Infinite M200). Glomelt dye showed maximum fluorescence initially, upon interacting with the exposed SNARE motifs of individual SNARE proteins. During trans-SNARE complex formation, a gradual decrease of fluorescence was observed as the dye was expelled out due to SNARE folding. For v-SNARE NDs, a fraction of t-SNAREs bound to v-SNAREs at a time  $t$  is given by  $1 - \frac{F_{\text{ND5} + \text{tSNARE liposome}}}{F_{\text{ND0} + \text{tSNARE liposome}}}$  and  $F_{\text{ND5} + \text{tSNARE liposome}}$  and  $F_{\text{ND0} + \text{tSNARE liposome}}$  are the corresponding fluorescence intensities at time  $t$  when t-SNARE liposomes reacted with ND5 (5 copies of syb2) and ND0 (no syb2), respectively. Similarly, for v-SNARE liposomes, a fraction of t-SNAREs bound to v-SNAREs at a time  $t$  is given by  $1 - \frac{F_{\text{vSNARE liposome} + \text{tSNARE liposome}}}{F_{\text{empty liposome} + \text{tSNARE liposome}}}$  and  $F_{\text{vSNARE liposome} + \text{tSNARE liposome}}$  and  $F_{\text{empty liposome} + \text{tSNARE liposome}}$  are the corresponding fluorescence intensities at time  $t$  when t-SNARE liposomes reacted with v-SNARE or empty liposomes, respectively. The presence of trans-SNARE complexes in the reaction mixtures was further confirmed by the immunoblots, using SNAP-25B-specific antibody. The v-SNARE density in NDs and liposomes used were similar in all the experiments above.

**Statistical Analysis.** The number of independent trials is provided in the figure legends, along with the statistical tests that were performed. Error bars represent SEM.

**Data Availability.** All study data are included in the article and/or supporting information.

**ACKNOWLEDGMENTS.** We thank Edwin R. Chapman, Meyer B. Jackson, Jayeeta Giri, Jason Vevea, and Das laboratory members for their suggestions and comments regarding this manuscript. This study was supported by a grant from the Department of Atomic Energy (Government of India) and Tata Institute of Fundamental Research-Mumbai (to D.D.).

1. M. H. Polymeropoulos *et al.*, Mutation in the alpha-synuclein gene identified in families with Parkinson's disease. *Science* **276**, 2045–2047 (1997).
2. R. Krüger *et al.*, Ala30Pro mutation in the gene encoding alpha-synuclein in Parkinson's disease. *Nat. Genet.* **18**, 106–108 (1998).
3. L. Maroteaux, J. T. Campanelli, R. H. Scheller, Synuclein: A neuron-specific protein localized to the nucleus and presynaptic nerve terminal. *J. Neurosci.* **8**, 2804–2815 (1988).
4. J. Lautenschläger, C. F. Kaminski, G. S. Kaminski Schierle,  $\alpha$ -synuclein - Regulator of exocytosis, endocytosis, or both? *Trends Cell Biol.* **27**, 468–479 (2017).
5. K. E. Larsen *et al.*, Alpha-synuclein overexpression in PC12 and chromaffin cells impairs catecholamine release by interfering with a late step in exocytosis. *J. Neurosci.* **26**, 11915–11922 (2006).
6. M. Ramezani *et al.*, Regulation of exocytosis and mitochondrial relocation by Alpha-synuclein in a mammalian cell model. *NPJ Parkinsons Dis.* **5**, 12 (2019).
7. S. M. Park *et al.*, Evidence that alpha-synuclein functions as a negative regulator of Ca(++)-dependent alpha-granule release from human platelets. *Blood* **100**, 2506–2514 (2002).
8. B. Gretten-Harrison *et al.*,  $\alpha\beta\gamma$ -synuclein triple knockout mice reveal age-dependent neuronal dysfunction. *Proc. Natl. Acad. Sci. U.S.A.* **107**, 19573–19578 (2010).
9. W. S. Davidson, A. Jonas, D. F. Clayton, J. M. George, Stabilization of alpha-synuclein secondary structure upon binding to synthetic membranes. *J. Biol. Chem.* **273**, 9443–9449 (1998).
10. J. Burré *et al.*, Alpha-synuclein promotes SNARE-complex assembly in vivo and in vitro. *Science* **329**, 1663–1667 (2010).
11. Y. Lai *et al.*, Nonaggregated  $\alpha$ -synuclein influences SNARE-dependent vesicle docking via membrane binding. *Biochemistry* **53**, 3889–3896 (2014).
12. X. Lou, J. Kim, B. J. Hawk, Y. K. Shin,  $\alpha$ -synuclein may cross-bridge v-SNARE and acidic phospholipids to facilitate SNARE-dependent vesicle docking. *Biochem. J.* **474**, 2039–2049 (2017).
13. J. Diao *et al.*, Native  $\alpha$ -synuclein induces clustering of synaptic-vesicle mimics via binding to phospholipids and synaptobrevin-2/VAMP2. *eLife* **2**, e00592 (2013).
14. V. M. Nemani *et al.*, Increased expression of alpha-synuclein reduces neurotransmitter release by inhibiting synaptic vesicle recluster after endocytosis. *Neuron* **65**, 66–79 (2010).
15. D. C. DeWitt, E. Rhoades,  $\alpha$ -synuclein can inhibit SNARE-mediated vesicle fusion through direct interactions with lipid bilayers. *Biochemistry* **52**, 2385–2387 (2013).
16. C. C. Huang *et al.*, Soluble  $\alpha$ -synuclein facilitates priming and fusion by releasing Ca<sup>2+</sup> from the thapsigargin-sensitive Ca<sup>2+</sup> pool in PC12 cells. *J. Cell Sci.* **131**, jcs213017 (2018).
17. T. Logan, J. Bendor, C. Toupin, K. Thorn, R. H. Edwards,  $\alpha$ -synuclein promotes dilation of the exocytotic fusion pore. *Nat. Neurosci.* **20**, 681–689 (2017).
18. M. Huang *et al.*,  $\alpha$ -synuclein: A multifunctional player in exocytosis, endocytosis, and vesicle recycling. *Front. Neurosci.* **13**, 28 (2019).
19. H. Bao *et al.*, Dynamics and number of trans-SNARE complexes determine nascent fusion pore properties. *Nature* **554**, 260–263 (2018).
20. D. Das, H. Bao, K. C. Courtney, L. Wu, E. R. Chapman, Resolving kinetic intermediates during the regulated assembly and disassembly of fusion pores. *Nat. Commun.* **11**, 231 (2020).
21. R. G. W. Staal, E. V. Mosharov, D. Sulzer, Dopamine neurons release transmitter via a flickering fusion pore. *Nat. Neurosci.* **7**, 341–346 (2004).
22. L. J. Breckenridge, W. Almers, Currents through the fusion pore that forms during exocytosis of a secretory vesicle. *Nature* **328**, 814–817 (1987).
23. T. Söllner *et al.*, SNAP receptors implicated in vesicle targeting and fusion. *Nature* **362**, 318–324 (1993).
24. S. Ferro-Novick, R. Jahn, Vesicle fusion from yeast to man. *Nature* **370**, 191–193 (1994).
25. H. Bao *et al.*, Exocytotic fusion pores are composed of both lipids and proteins. *Nat. Struct. Mol. Biol.* **23**, 67–73 (2016).
26. T. Weber *et al.*, SNAREpins: Minimal machinery for membrane fusion. *Cell* **92**, 759–772 (1998).
27. J. A. McNew *et al.*, Compartmental specificity of cellular membrane fusion encoded in SNARE proteins. *Nature* **407**, 153–159 (2000).
28. M. Lindau, W. Almers, Structure and function of fusion pores in exocytosis and ectoplasmic membrane fusion. *Curr. Opin. Cell Biol.* **7**, 509–517 (1995).
29. C. W. Chang, C. W. Chiang, M. B. Jackson, Fusion pores and their control of neurotransmitter and hormone release. *J. Gen. Physiol.* **149**, 301–322 (2017).
30. J. Rizo, J. Xu, The synaptic vesicle release machinery. *Annu. Rev. Biophys.* **44**, 339–367 (2015).
31. R. J. Perrin, W. S. Woods, D. F. Clayton, J. M. George, Interaction of human alpha-synuclein and Parkinson's disease variants with phospholipids. Structural analysis using site-directed mutagenesis. *J. Biol. Chem.* **275**, 34393–34398 (2000).
32. S. Chandra, X. Chen, J. Rizo, R. Jahn, T. C. Südhof, A broken alpha-helix in folded alpha-synuclein. *J. Biol. Chem.* **278**, 15313–15318 (2003).
33. U. Kaur, J. C. Lee, Unroofing site-specific  $\alpha$ -synuclein-lipid interactions at the plasma membrane. *Proc. Natl. Acad. Sci. U.S.A.* **117**, 18977–18983 (2020).
34. J. Sun *et al.*, Functional cooperation of  $\alpha$ -synuclein and VAMP2 in synaptic vesicle recycling. *Proc. Natl. Acad. Sci. U.S.A.* **116**, 11113–11115 (2019).
35. E. R. Chapman, How does synaptotagmin trigger neurotransmitter release? *Annu. Rev. Biochem.* **77**, 615–641 (2008).
36. N. Brose, A. G. Petrenko, T. C. Südhof, R. Jahn, Synaptotagmin: A calcium sensor on the synaptic vesicle surface. *Science* **256**, 1021–1025 (1992).
37. C. Ma, L. Su, A. B. Seven, Y. Xu, J. Rizo, Reconstitution of the vital functions of Munc18 and Munc13 in neurotransmitter release. *Science* **339**, 421–425 (2013).
38. J. Jiao *et al.*, Munc18-1 catalyzes neuronal SNARE assembly by templating SNARE association. *eLife* **7**, e41771 (2018).
39. E. A. Prinslow, K. P. Stepien, Y. Z. Pan, J. Xu, J. Rizo, Multiple factors maintain assembled trans-SNARE complexes in the presence of NSF and  $\alpha$ -SNAP. *eLife* **8**, e38880 (2019).
40. M. C. Chicka, E. Hui, H. Liu, E. R. Chapman, Synaptotagmin arrests the SNARE complex before triggering fast, efficient membrane fusion in response to Ca<sup>2+</sup>. *Nat. Struct. Mol. Biol.* **15**, 827–835 (2008).
41. N. A. Courtney, H. Bao, J. S. Briguglio, E. R. Chapman, Synaptotagmin 1 clamps synaptic vesicle fusion in mammalian neurons independent of complexin. *Nat. Commun.* **10**, 4076 (2019).
42. L. Shi *et al.*, SNARE proteins: One to fuse and three to keep the nascent fusion pore open. *Science* **335**, 1355–1359 (2012).
43. L. Shi *et al.*, Preparation and characterization of SNARE-containing nanodiscs and direct study of cargo release through fusion pores. *Nat. Protoc.* **8**, 935–948 (2013).
44. M. M. Bradberry *et al.*, Molecular basis for synaptotagmin-1-associated neurodevelopmental disorder. *Neuron* **107**, 52–64.e7 (2020).
45. B. Antony, Mechanisms of membrane curvature sensing. *Annu. Rev. Biochem.* **80**, 101–123 (2011).
46. T. S. Strutzenberg *et al.*, HDX-MS reveals structural determinants for ROR gamma hyperactivation by synthetic agonists. *eLife* **8**, e47172 (2019).
47. W. C. Tucker, T. Weber, E. R. Chapman, Reconstitution of Ca<sup>2+</sup>-regulated membrane fusion by synaptotagmin and SNAREs. *Science* **304**, 435–438 (2004).
48. S. Takamori *et al.*, Molecular anatomy of a trafficking organelle. *Cell* **127**, 831–846 (2006).
49. R. Sinha, S. Ahmed, R. Jahn, J. Klingauf, Two synaptobrevin molecules are sufficient for vesicle fusion in central nervous system synapses. *Proc. Natl. Acad. Sci. U.S.A.* **108**, 14318–14323 (2011).
50. N. Wu, P. R. Joshi, C. Cepeda, E. Masliah, M. S. Levine, Alpha-synuclein overexpression in mice alters synaptic communication in the corticostriatal pathway. *J. Neurosci. Res.* **88**, 1764–1776 (2010).
51. S. Janežic *et al.*, Deficits in dopaminergic transmission precede neuron loss and dysfunction in a new Parkinson model. *Proc. Natl. Acad. Sci. U.S.A.* **110**, E4016–E4025 (2013).
52. S. Liu *et al.*, alpha-synuclein produces a long-lasting increase in neurotransmitter release. *EMBO J.* **23**, 4506–4516 (2004).
53. J. B. Watson *et al.*, Alterations in corticostriatal synaptic plasticity in mice overexpressing human alpha-synuclein. *Neuroscience* **159**, 501–513 (2009).
54. S. Chandra *et al.*, Double-knockout mice for alpha- and beta-synucleins: Effect on synaptic functions. *Proc. Natl. Acad. Sci. U.S.A.* **101**, 14966–14971 (2004).
55. S. L. Senior *et al.*, Increased striatal dopamine release and hyperdopaminergic-like behaviour in mice lacking both alpha-synuclein and gamma-synuclein. *Eur. J. Neurosci.* **27**, 947–957 (2008).
56. S. Anwar *et al.*, Functional alterations to the nigrostriatal system in mice lacking all three members of the synuclein family. *J. Neurosci.* **31**, 7264–7274 (2011).
57. B. Quade *et al.*, Membrane bridging by Munc13-1 is crucial for neurotransmitter release. *eLife* **8**, e42806 (2019).
58. Z. P. P. Pang, T. C. Südhof, Cell biology of Ca<sup>2+</sup>-triggered exocytosis. *Curr. Opin. Cell Biol.* **22**, 496–505 (2010).
59. J. B. Sørensen, R. Fernández-Chacón, T. C. Südhof, E. Neher, Examining synaptotagmin 1 function in dense core vesicle exocytosis under direct control of Ca<sup>2+</sup>. *J. Gen. Physiol.* **122**, 265–276 (2003).
60. P. S. Pinheiro, S. Houy, J. B. Sørensen, C2-domain containing calcium sensors in neuroendocrine secretion. *J. Neurochem.* **139**, 943–958 (2016).
61. H. Bernheimer, W. Birkmayer, O. Hornykiewicz, K. Jellinger, F. Seitelberger, Brain dopamine and the syndromes of Parkinson and Huntington. Clinical, morphological and neurochemical correlations. *J. Neurol. Sci.* **20**, 415–455 (1973).
62. E. Maries, B. Dass, T. J. Collier, J. H. Kordower, K. Steece-Collier, The role of alpha-synuclein in Parkinson's disease: Insights from animal models. *Nat. Rev. Neurosci.* **4**, 727–738 (2003).
63. C. G. Schuette *et al.*, Determinants of liposome fusion mediated by synaptic SNARE proteins. *Proc. Natl. Acad. Sci. U.S.A.* **101**, 2858–2863 (2004).
64. J. Burré, M. Sharma, T. C. Südhof,  $\alpha$ -synuclein assembles into higher-order multimers upon membrane binding to promote SNARE complex formation. *Proc. Natl. Acad. Sci. U.S.A.* **111**, E4274–E4283 (2014).
65. J. Xu *et al.*, Mechanistic insights into neurotransmitter release and presynaptic plasticity from the crystal structure of Munc13-1 C<sub>1</sub>C<sub>2</sub>BMUN. *eLife* **6**, e22567 (2017).
66. D. A. Archer, M. E. Graham, R. D. Burgoyne, Complexin regulates the closure of the fusion pore during regulated vesicle exocytosis. *J. Biol. Chem.* **277**, 18249–18252 (2002).
67. J. Tang *et al.*, A complexin/synaptotagmin 1 switch controls fast synaptic vesicle exocytosis. *Cell* **126**, 1175–1187 (2006).
68. M. Itakura, H. Misawa, M. Sekiguchi, S. Takahashi, M. Takahashi, Transfection analysis of functional roles of complexin I and II in the exocytosis of two different types of secretory vesicles. *Biochem. Biophys. Res. Commun.* **265**, 691–696 (1999).
69. J. R. Schaub, X. Lu, B. Doneske, Y. K. Shin, J. A. McNew, Hemifusion arrest by complexin is relieved by Ca<sup>2+</sup>-synaptotagmin I. *Nat. Struct. Mol. Biol.* **13**, 748–750 (2006).
70. T. J. Melia Jr, Putting the clamps on membrane fusion: How complexin sets the stage for calcium-mediated exocytosis. *FEBS Lett.* **581**, 2131–2139 (2007).
71. Z. Wang, H. Liu, Y. Gu, E. R. Chapman, Reconstituted synaptotagmin I mediates vesicle docking, priming, and fusion. *J. Cell Biol.* **195**, 1159–1170 (2011).
72. A. E. Powers, D. S. Patel, Expression and purification of untagged  $\alpha$ -synuclein. *Methods Mol. Biol.* **1948**, 261–269 (2019).
73. R. Cappai *et al.*, Dopamine promotes alpha-synuclein aggregation into SDS-resistant soluble oligomers via a distinct folding pathway. *FASEB J.* **19**, 1377–1379 (2005).
74. B. K. Choi *et al.*, Large  $\alpha$ -synuclein oligomers inhibit neuronal SNARE-mediated vesicle docking. *Proc. Natl. Acad. Sci. U.S.A.* **110**, 4087–4092 (2013).
75. P. Mueller, D. O. Rudin, H. T. Tien, W. C. Westcott, Reconstitution of cell membrane structure in vitro and its transformation into an excitable system. *Nature* **194**, 979–980 (1962).
76. A. Finkelstein, Bilayers: Formation, measurements, and incorporation of components. *Methods Enzymol.* **32**, 489–501 (1974).
77. H. Akaike, A new look at the statistical model identification. *IEEE Trans. Automat. Contr.* **19**, 716–723 (1974).
78. D. Das, B. A. Krantz, Peptide- and proton-driven allosteric clamps catalyze anthrax toxin translocation across membranes. *Proc. Natl. Acad. Sci. U.S.A.* **113**, 9611–9616 (2016).